Atmos. Chem. Phys., 11, 1791–1811, 2011
www.atmos-chem-phys.net/11/1791/2011/
doi:10.5194/acp-11-1791-2011

Atmospheric Chemistry and Physics

Global observations of tropospheric BrO columns using GOME-2 satellite data

N. Theys[1], M. Van Roozendael[1], F. Hendrick[1], X. Yang[2,3], I. De Smedt[1], A. Richter[4], M. Begoin[4], Q. Errera[1], P. V. Johnston[5], K. Kreher[5], and M. De Mazière[1]

[1]Belgian Institute for Space Aeronomy (IASB-BIRA), Brussels, Belgium
[2]National Centre for Atmospheric Science (NCAS), Cambridge, CB2 1EW, UK
[3]Centre for Atmospheric Science, Department of Chemistry, University of Cambridge, Cambridge CB2 1EW, UK
[4]Institute of Environmental Physics, University of Bremen, Bremen, Germany
[5]National Institute of Water and Atmospheric Research (NIWA), Omakau, Central Otago, New Zealand

Received: 8 October 2010 – Published in Atmos. Chem. Phys. Discuss.: 22 November 2010
Revised: 17 February 2011 – Accepted: 20 February 2011 – Published: 25 February 2011

Abstract. Measurements from the GOME-2 satellite instrument have been analyzed for tropospheric BrO using a residual technique that combines measured BrO columns and estimates of the stratospheric BrO content from a climatological approach driven by O_3 and NO_2 observations. Comparisons between the GOME-2 results and BrO vertical columns derived from correlative ground-based and SCIAMACHY nadir observations, present a good level of consistency. We show that the adopted technique enables separation of stratospheric and tropospheric fractions of the measured total BrO columns and allows quantitative study of the BrO plumes in polar regions. While some satellite observed plumes of enhanced BrO can be explained by stratospheric descending air, we show that most BrO hotspots are of tropospheric origin, although they are often associated to regions with low tropopause heights as well. Elaborating on simulations using the *p*-TOMCAT tropospheric chemical transport model, this result is found to be consistent with the mechanism of bromine release through sea salt aerosols production during blowing snow events. No definitive conclusion can be drawn however on the importance of blowing snow sources in comparison to other bromine release mechanisms. Outside polar regions, evidence is provided for a global tropospheric BrO background with column of 1–3 $\times 10^{13}$ molec cm^{-2}, consistent with previous estimates.

Correspondence to: N. Theys
(theys@aeronomie.be)

1 Introduction

Inorganic bromine (Br_y = Br + BrO + $BrONO_2$ + HOBr + HBr + BrCl) is known to play an important role in the chemistry of the stratosphere. Bromine monoxide (BrO) is responsible for ozone depletion through catalytic reactions with NO_2, ClO, HO_2 and O (Lary, 1996). In spite of the small quantities of Br_y in the stratosphere, it contributes to mid-latitude ozone loss by about 25% and for polar ozone depletion, mostly through the BrO/ClO cycle (McElroy et al., 1986), up to 50%. The main sources of Br_y in the stratosphere are long-lived organic bromine compounds (CH_3Br, $CBrClF_2$, $CBrF_3$, $CBrF_2CBrF_2$), mostly of anthropogenic origin, which contribute to the stratospheric Br_y loading by about 16–17 parts per trillion volume (pptv) (Montzka et al., 2003). However, several measurements of stratospheric BrO using remote-sensing UV-visible techniques have inferred a total Br_y loading of 18–25 pptv, suggesting that an additional contribution must be considered, possibly due to the bromine release from short-lived biogenic organic compounds (e.g., $CHBr_3$, CH_2Br_2)or even through direct injection of tropospheric Br_y into the lower stratosphere (WMO, 2007, and references therein; Salawitch et al., 2010).

After the role of bromine in the destruction of stratospheric ozone was highlighted, it became soon clear that inorganic bromine compounds could also have a significant effect in the troposphere (for an overview see, e.g., von Glasow and Crutzen, 2007). In the boundary layer, it was found that large amounts of inorganic bromine are seasonally released in polar region in both hemispheres during spring (e.g., Hausmann and Platt, 1994; Kreher et al., 1997; Wagner and Platt, 1998; Richter et al., 1998; Chance, 1998; Sirois and Barrie, 1999; Hönninger and Platt, 2002; Frieß et al., 2004) due

to a phenomenon known as polar bromine explosion that involves the release of bromine from sea salt to the gas phase through a sequence of autocatalytic photochemical and heterogeneous reactions (a review is provided in Simpson et al., 2007). However, the mechanism for the bromine release during bromine explosions is not completely understood. The surfaces needed for reactions can potentially come from frost flowers (Kaleschke et al., 2004), fresh sea ice (Frieß et al., 2004), sea salt aerosols (Vogt et al., 1996), sea salt deposits (McConnell et al., 1992) or sea salt aerosols produced during blowing snow events (Yang et al., 2008 and 2010; Jones et al., 2009 and 2010). In any case, the occurrence of such bromine emissions leads to efficient ozone depletion in the polar troposphere (e.g., Wennberg, 1999), as well as interactions with mercury chemistry (Schroeder et al., 1998).

Although more localized, inorganic bromine emissions have also been identified over salt lakes (Hebestreit et al., 1999), in the marine boundary layer (Leser et al., 2003; Saiz-Lopez et al., 2004; Read et al., 2008) and in volcanic plumes (Bobrowski et al., 2003; Oppenheimer et al., 2006; Theys et al., 2009a). Observations from space (e.g., Richter et al., 2002; Van Roozendael et al., 2002), ground-based (Hendrick et al., 2007; Theys et al., 2007) and balloon-borne (Harder et al., 1998; Fitzenberger et al., 2000) instruments have shown that inorganic bromine may be produced and sustained in the free troposphere at the global scale. Elaborating on these observations, modelling results (von Glasow et al., 2004; Lary, 2005; Yang et al., 2005, 2010) have shown that free-tropospheric bromine might have a significant impact on the tropospheric ozone budget (and on tropospheric chemistry in general), leading to a reduction in the O_3 mixing ratio of up to 40% locally.

Satellite UV-visible nadir instruments, such as GOME/ERS-2, SCIAMACHY/ENVISAT, GOME-2/MetOp-A and OMI/Aura, offer the unique capability to study and monitor BrO at the global scale (Chance, 1998; Richter et al., 1998, 2002; Van Roozendael et al., 2002; Wagner and Platt, 1998). However, a quantitative and refined interpretation of the satellite BrO observations requires to resolve the measured total BrO columns into their stratospheric and tropospheric contributions. In past studies (e.g., Wagner and Platt, 1998; Richter et al., 1998; Hollwedel, 2005), this troposphere-stratosphere separation has been treated only on limited case studies. Generally, the tropospheric BrO column was derived by subtracting from the measured total column, a stratospheric column estimated from the satellite nadir measurements at the same latitude over a certain geographical sector or at high solar zenith angle (corresponding to high latitude). This implies several assumptions, in particular: (1) a negligible impact of the tropospheric BrO content on the stratospheric correction, and (2) a weak longitudinal or latitudinal dependence of the stratospheric BrO column. However, these hypotheses are questionable because of the possible overall presence of BrO in the troposphere and the longitudinal and latitudinal inhomogeneity of stratospheric BrO. The latter point is crucial as it has recently been argued that the stratospheric BrO column variability could be larger than previously thought, being exacerbated by the supply of significant amounts of Br_y in the lower stratosphere from short-lived bromocarbons (Salawitch et al., 2010). One possibility to estimate stratospheric BrO columns at the global scale is to use the BrO profiles measured by the SCIAMACHY instrument in its limb mode (see e.g. Sinnhuber et al., 2005). Although these profiles are of excellent quality (Hendrick et al., 2009), their use to retrieve tropospheric BrO columns is limited to SCIAMACHY data. Moreover, the retrieval of stratospheric BrO profiles from SCIAMACHY limb observations is most of the time only possible in the altitude range from about 15 km to 30 km.

In a previous paper (Theys et al., 2009b), we have developed and validated a new stratospheric BrO climatology that accounts for the important dynamical and photochemical variations of stratospheric BrO. The main motivation was to use it as stratospheric correction in the retrieval of tropospheric BrO columns from satellite nadir observations. We now apply it to GOME-2 measurements obtained in 2007 and 2008. We have developed an advanced algorithm to retrieve tropospheric BrO columns that treats the changes in measurement vertical sensitivity in both troposphere and stratosphere due to clouds, surface reflectivity and viewing geometry. Our method enables to separate the large-scale stratospheric and tropospheric BrO structures in the total BrO column field measured from space. It allows to better study the polar tropospheric BrO hotspots and also to further investigate the existence of a free-tropospheric BrO background at the global scale.

2 Instrument

The second Global Ozone Monitoring Experiment (GOME-2) is a UV/visible spectrometer covering the 240–790 nm wavelength interval with a spectral resolution of 0.2–0.5 nm (Munro et al., 2006). GOME-2 measures the solar radiation backscattered by the atmosphere and reflected from the surface of the Earth in a nadir viewing geometry. A solar spectrum is also measured via a diffuser plate once per day. The ground pixel size is $80 \times 40\,km^2$ and the full width of a normal GOME-2 scanning swath is 1920 km. Global coverage is achieved within 1.5–3 days at the equator and within one day poleward of $\pm 45°$ latitude. The GOME-2 instrument was launched on board the Meteorological Operational satellite-A (MetOp-A) in October 2006. The MetOp-A satellite is in a sun-synchronous polar orbit with an equator crossing time of 09:30 LT on the descending node.

The main objective of GOME-2 is the global monitoring of the total ozone field. However, the good spectral resolution and coverage of the instrument also allows for the retrieval of a number of other absorbing trace gases such as NO_2, SO_2,

H_2CO, CHOCHO, OClO, H_2O and BrO, as well as cloud and aerosol parameters.

3 Data analysis

In this work, the tropospheric BrO vertical column densities (VCD_{tropo}) are retrieved using a residual technique (see e.g., Boersma et al., 2004) according to the following equation:

$$VCD_{tropo} = \frac{SCD - VCD_{strato}.AMF_{strato}}{AMF_{tropo}} \quad (1)$$

The approach consists of three main steps:

1. A slant column density (SCD) is determined from calibrated earth-shine and irradiance spectra using a DOAS fit, as further explained in Sect. 3.1. This slant column is a "total" SCD in the sense that it includes contributions from absorption by BrO in both the stratosphere and troposphere.

2. The stratospheric vertical column (VCD_{strato}) is estimated using simulated stratospheric BrO profiles. Details are given in Sect. 3.2.

3. The residual tropospheric vertical column is obtained by applying stratospheric and tropospheric air mass factors (AMF_{strato} and AMF_{tropo}) to account for changes in measurement sensitivity in both stratospheric and tropospheric layers. This aspect is presented in Sect. 3.3.

An error analysis of the tropospheric BrO vertical columns is then given in Sect. 3.4.

3.1 DOAS slant column retrieval

The measured spectra are analysed with the Differential Optical Absorption Spectroscopy (DOAS) technique (Platt and Stutz, 2008). Atmospheric absorbers (in particular BrO) are separated using the characteristic differential structures of their absorption cross-sections determined from laboratory measurements. The retrieved quantity can be regarded as the integrated BrO concentration along the mean optical light path (it is often referred to as the "slant column density"). Here, the spectral evaluation consists of a least-squares fit procedure where cross-sections of BrO (223 K) (Fleischman et al., 2004), ozone (228 K and 243 K) (Brion et al., 1993), NO_2 (243 K) (Burrows et al., 1998), H_2CO (297 K) (Meller et al., 2000) and OClO (293 K) (Bogumil et al., 2003) are adjusted to the log-ratio of a measured and a reference spectrum (the latest solar spectrum measured by the instrument). The absorption cross-sections are convolved using the GOME-2 instrumental slit function (Siddans et al., 2006) and they are corrected for the solar I_0 effect (Aliwell et al., 2002). The residual broadband features due to Rayleigh and Mie scattering are removed using a fifth order closure polynomial. A linear offset correction is also applied. To correct for the Ring effect (Grainger and Ring, 1962), two pseudo absorption cross-sections generated after Vountas et al. (1998) using the SCIATRAN radiative transfer model (Rozanov et al., 2001) are included in the fit. Furthermore, two spectra are included in the fit, to account for the response of the instrument to the polarization of the incoming light (EUMETSAT, GOME-2 FM-203 Calibration Key data, Eta and Zeta).

An important difference in the BrO DOAS settings presented here with respect to our previous study (Theys et al., 2009a) relies in the choice of the fitting window which has been extended towards shorter wavelengths (332–359 nm) in order to cover five BrO absorption bands. While the BrO values retrieved using both fitting windows are consistent above regions of enhanced tropospheric BrO precursors emissions, the use of this extended wavelength interval leads to an overall reduction of the noise of the slant columns and allows minimising the impact of several well-known artefacts: a spurious slant column viewing angle dependence, the presence in the measurement maps of cloud structures due to imperfect correction of the Ring effect and a strong interference with formaldehyde absorption over regions heavily polluted or affected by biomass burning or biogenic emission. This is illustrated in Fig. 1. In order to better cope with the enhanced ozone absorption at wavelengths shorter than 336 nm, an AMF-modified DOAS approach (Richter, 1997) has been adopted. This considers the product of the wavelength dependent ozone AMFs and the ozone absorption cross-sections in the DOAS analysis rather than the ozone cross-sections alone. The wavelength ozone AMFs used in the present analysis have been calculated for different representative solar zenith angles (SZA) and for a mid-latitudinal ozone profile corresponding to a total column of 450 Dobson units. Note that for SZA lower than 90° the results are only weakly dependent on the ozone profile and column used in the retrieval.

An example of a BrO fit to GOME-2 data is shown in Fig. 2 for a tropospheric BrO event. It can be seen that the inclusion of five BrO absorption bands in the fit yields an unambiguous detection of BrO.

3.2 Stratospheric BrO correction

The stratospheric BrO profiles are estimated using the dynamical climatology of BrO profiles extensively described in Theys et al. (2009b). The climatology is based on the output of the 3-D chemical transport model BASCOE (Errera et al., 2008; Viscardy et al., 2010) which has been optimized for bromine photochemistry and budget. The total stratospheric inorganic bromine loading is of 23 pptv – including a contribution of 6 pptv by brominated very short-lived substances. Modelled BrO profiles have been validated through comparisons using a large dataset of ground-based, balloon-borne, and satellite limb stratospheric BrO observations (Theys et al., 2009b). The climatology is based on a parameterization

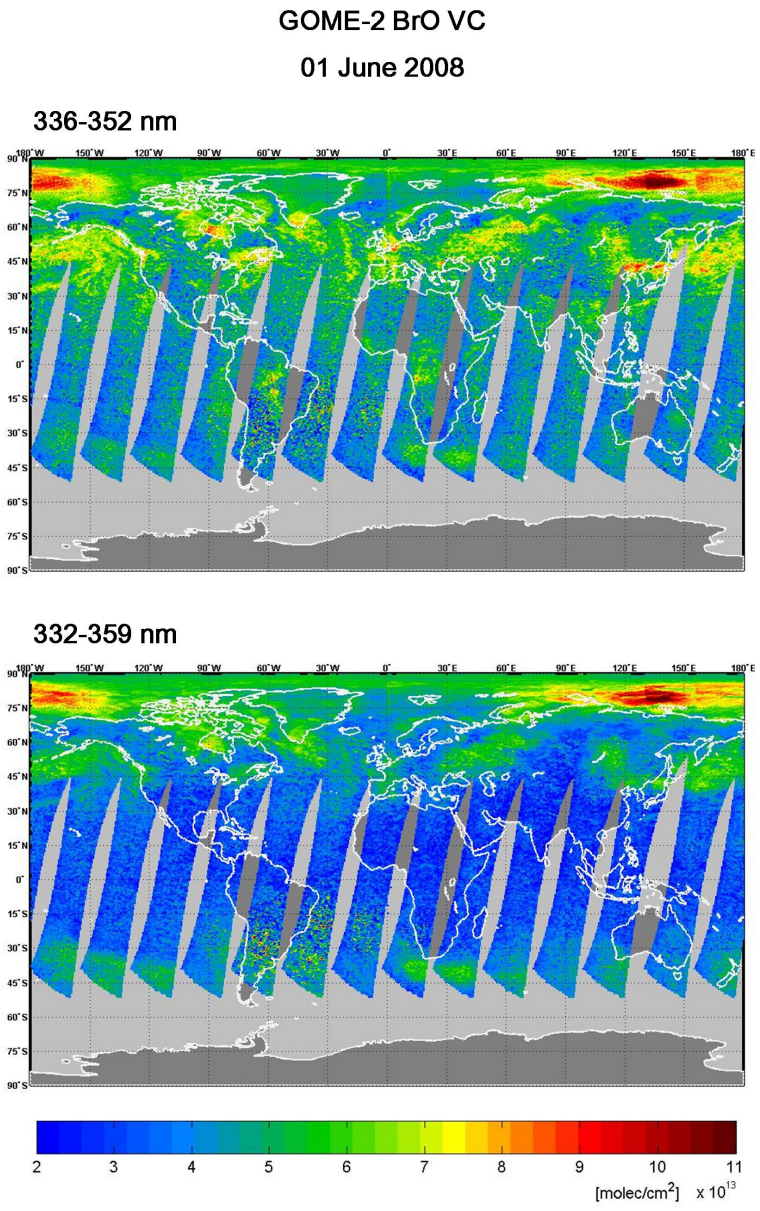

Fig. 1. Comparison of GOME-2 BrO vertical columns for 1 June 2008 using (upper map) the 336–352 nm fitting window from Theys et al. (2009a) and (lower map) the 332–359 nm interval introduced in this study. Simple geometrical air mass factors have been used to convert BrO slant columns into vertical columns. Note the reduced artefacts due to formaldehyde interference (e.g., in East China or Central Africa), the elimination of the viewing angle dependence and the reduced cloud-related structures.

using dynamical and chemical indicators. The impact of the atmospheric dynamics on the stratospheric BrO distribution is treated by means of Br_y/ozone correlations, while photochemical effects are taken into account using stratospheric NO_2 columns as an indicator of the BrO/Br_y ratio (see e.g., Lary, 1996). In practice, for each sounded pixel, a stratospheric BrO profile is calculated from the parameterization using the O_3 and NO_2(stratospheric) vertical columns retrieved by the Deutsches Zentrum für Luft- und Raumfahrt (DLR, level-2 operational product, GDP 4.3) from the same GOME-2 measurement. This approach is convenient since it requires only limited computational resources. Moreover, as the climatology uses measured quantities to evaluate stratospheric BrO, it guarantees that the sounded air masses and geophysical conditions are optimally represented.

The stratospheric BrO vertical columns are derived by integrating simulated stratospheric BrO profiles between the tropopause and the top-of-atmosphere. The tropopause is calculated using the potential vorticity (PV) determined on isentropic levels from meteorological data of the European

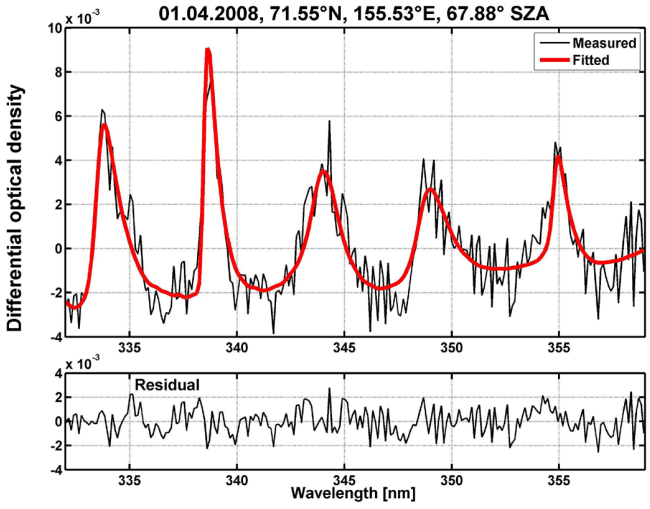

Fig. 2. Example of a fit to the measured BrO differential absorption in the 332–359 nm wavelength interval during a tropospheric BrO event. The slant column is 6.14×10^{14} molec cm^{-2}.

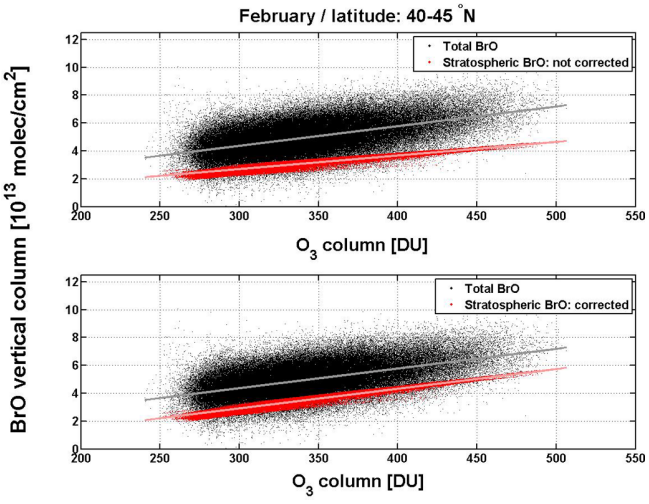

Fig. 3. Illustration of the adjustment procedure used to bring the stratospheric BrO climatology in close agreement with GOME-2 measurements for the Northern Hemisphere (February (40–45° N)). After adjustment, the slope of the regression line between the stratospheric BrO VCDs and the O_3 VCDs (light red line) is equal to the slope of the regression line through the scatterplot between the measured total BrO VCDs and the O_3 VCDs (grey line). Note that the total BrO columns are calculated using stratospheric air mass factors.

Centre for Medium-Range Weather Forecasts (ECMWF) sampled on a $1° \times 1°$ latitude-longitude grid (ERA-Interim analysis). The tropopause height is defined by the 3.5 PVU contour (1 PVU = 10^{-6} m^2 K s^{-1} kg^{-1}), joined to the 380 K isentropic surface in the tropics where the 3.5 PVU contour rises above this level. This so-called dynamical tropopause agrees reasonably well with the thermal tropopause, defined in terms of the temperature lapse rate by the World Meteorological Organization (WMO), despite a general tendency to give a tropopause lower by 1 km on average (Schoeberl, 2004), with a small effect on the stratospheric BrO column calculation (maximum 3% differences). We have decided to use the dynamical tropopause height rather than the thermal tropopause essentially because the latter is generally undefined for typical Antarctic ozone hole conditions (where the condition dT/dz > -2K/km is often encountered only in the stratosphere above 15 km altitude). In a last step, a fine adjustment of the climatology is performed to ensure consistency with GOME-2 measurements. The approach is similar in concept to the correction used for the retrieval of tropospheric NO_2 columns by Richter et al. (2005). Here the correction is based on the fact that the variations in stratospheric Br_y are controlled by atmospheric dynamics in a way that matches closely the O_3 fluctuations, as clearly established by Theys et al. (2009b) and further demonstrated by Salawitch et al. (2010) using measured O_3 and BrO vertical columns. We assume that in conditions described below the slope of a BrO versus O_3 regression plot is fully controlled by stratospheric BrO. The correction then consists in adjusting the slope of the modelled BrO/O_3VCD correlation plot to the measured total BrO/O_3 VCD. In this procedure, the modelled and measured total BrO vertical columns are collected for two mid-latitudinal bands (40–45° N and 40–45° S, to construct separate correction for the Northern and Southern Hemispheres). In order to best constrain the slope of the scatter plots, we have considered the data for the months of February and August (for the corrections of the Northern and Southern Hemispheres, respectively) as on the one hand, a large variability in O_3 columns is observed at mid-latitudes for these months (due to strong dynamical changes of the stratosphere), and on the other hand, possible contamination of the measurements by elevated boundary layer BrO (e.g., transported from the polar region) is negligible. Note that the correction described here uses a slope adjustment but leaves unchanged any possible offset between modelled and measured total BrO VCD. Hence it preserves the information on the BrO background (not correlated with ozone) presumably present in the free-troposphere. This is achieved by keeping fixed the point at 250 DU of the modelled (adjusted) regression line, which reflects the fact that the discrepancy between the modelled and the measured BrO columns is likely to be larger for high O_3 columns. An illustration of the Northern Hemisphere correction is given in Fig. 3.

3.3 Air mass factors calculation

The air mass factor is defined by the ratio of the slant column to the vertical column (AMF = SCD/VCD). In this study the air mass factors are calculated under the assumption of optically thin atmospheric absorbers. For these conditions,

the scattering weight formulation introduced by Palmer et al. (2001) can be used:

$$\mathrm{AMF} = \int WF(z)N(z)dz \quad (2)$$

In this expression, $N(z)$ is the concentration profile of the atmospheric species of interest normalized by the corresponding vertical column and *WF(z)* is the so-called weighting function (no unit) that contains the dependences on all the parameters influencing the AMF, except the vertical profile of the species $N(z)$. The stratospheric and tropospheric air mass factors are estimated by integrating Eq. (2) over the altitude ranges of interest (from the surface to the tropopause, and from the tropopause to the top-of-atmosphere, respectively) using stratospheric (Sect. 3.2) and tropospheric (Sect. 3.3.3) BrO profiles, respectively. The weighting function depends on the observation geometry and on the scattering properties of the atmosphere and the surface. In this work, WFs have been evaluated from radiative transfer calculations performed with the pseudo-spherical multiple scattering UVSpec/DISORT code (Mayer and Killing, 2005). WFs have been modelled for a number of representative viewing geometries (solar zenith angles, viewing zenith angles and relative azimuth angles), surface albedos and ground altitudes, and stored in a look-up-table. Calculations are made at 345.5 nm, i.e. the centre wavelength of the fitting interval used. Sensitivity tests have been carried out in order to estimate the wavelength dependency of the calculated air mass factors within the fitting interval (332–359 nm). Results from these sensitivity tests show that using the centre wavelength of the interval (345.5 nm) leads to errors on the AMFs that are smaller than 5%, except for low sun conditions (solar zenith angles larger than 85°, not considered in our retrieval).

3.3.1 Impacts of clouds and surface albedo

The treatment of partially cloudy pixels (characterized by an effective cloud fraction area f) is based on the hypothesis of the "independent pixel approximation". It is assumed that the intensity measured by the instrument is the sum of the intensities of a completely clear and a completely cloudy pixel weighted by $(1-f)$ and f respectively. Under such circumstances, the weighting function for a partially cloudy scene is given by (Martin et al., 2002):

$$WF(z) = \Phi \cdot WF_{\mathrm{cloud}}(z) + (1-\Phi) \cdot WF_{\mathrm{clear}}(z) \quad (3)$$

where $WF_{\mathrm{cloud}}(z)$ is the weighting function for a completely cloudy scene, and $WF_{\mathrm{clear}}(z)$ is the weighting function for a corresponding cloud-free pixel. Φ is the intensity-weighted cloud fraction:

$$\Phi = \frac{f I_{\mathrm{cloud}}}{f I_{\mathrm{cloud}} + (1-f) I_{\mathrm{clear}}} \quad (4)$$

I_{cloud} and I_{clear} being the backscattered intensities for fully cloudy and clear scenes, respectively. The variables in Eq. (3) are estimated using the cloud fraction retrieved by the FRESCO+ algorithm (Wang et al., 2008) and by considering two Lambertian reflectors consistent with the FRESCO+ settings: one reflector representing the cloud at the retrieved cloud top pressure (albedo: 0.8) and the other one representing the surface with an albedo taken from the climatology of Koelemeijer et al. (2003) but at a wavelength of 335 nm (more in line with the wavelengths used to retrieve the BrO slant columns). To minimize the bias resulting from clouds, the analysis includes only the measurements with a cloud fraction below 0.4 and with a pressure difference between the surface and the top of the cloud less than 400 mbar. Note that no explicit correction is applied for aerosols but the cloud correction scheme accounts for a large part of the aerosol scattering effect (Boersma et al., 2004).

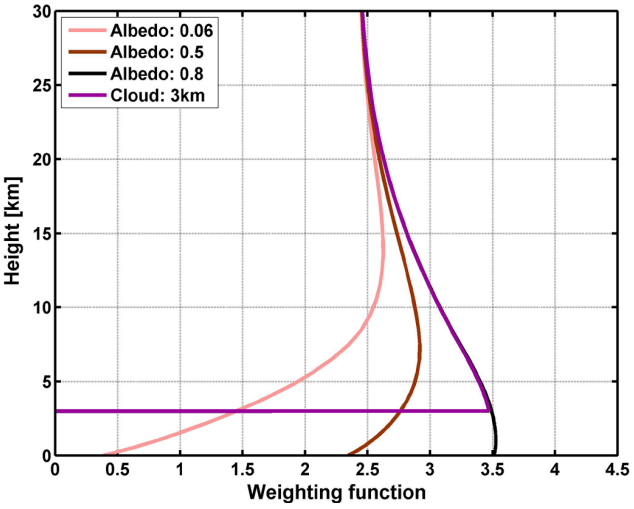

Fig. 4. Satellite weighting functions at 345.5 nm as function of surface albedo (0.06, 0.5 and 0.8 for a surface at sea level) and for a fully cloudy scene (cloud top height: 3 km, cloud albedo: 0.8). Calculations are made for a pure nadir observation geometry (line-of-sight angle: 0°) and a solar zenith angle of 45°.

An illustration of the weighting functions ($WF_{\mathrm{clear}}(z)$ and $WF_{\mathrm{cloud}}(z)$) is given in Fig. 4, for a clear-sky case with a surface altitude of 0 km (assuming a surface albedo of 0.06, 0.5 and 0.8) and for a cloudy case with a cloud top height of 3 km. It shows the typical behaviour of the satellite nadir UV measurement sensitivity to an absorber located at different altitudes for various surface albedo situations and for a totally cloudy scene.

3.3.2 Treatment of snow/ice-covered surfaces

Surfaces covered by snow or ice are of particular importance for the retrieval of tropospheric BrO columns since the large concentrations of BrO in the polar boundary layer are generally observed over bright surfaces. Unfortunately, FRESCO+ is unable to derive an effective cloud fraction for high albedo scenes, because this fraction is basically determined from the

contrast of the cloud with respect to the underlying surface. Nevertheless, we exploit the FRESCO + data in the snow/ice dedicated mode by considering the retrieved cloud top pressure and albedo as representative of the sounded surface and by using these Lambertian surface properties to calculate the WFs. Only scenes for which the difference between the surface pressure and the retrieved cloud top pressure is below 120 mbar are considered, so that pixels contaminated by thick elevated clouds are eliminated from the analysis.

A special case has also been designed for the fresh snow scenes: as the snow/ice mode of FRESCO+ is triggered by a monthly-averaged albedo database, pixels covered by fresh snow are not detected in this mode, but are considered as cloudy pixels in the nominal mode of FRESCO+. Hence, to account for these fresh snow scenes, we include in the analysis the pixels with a cloud fraction larger than 0.7 and with a pressure difference between the surface and the top of the "cloud" smaller than 150 mbar.

3.3.3 Tropospheric BrO profile shape

Since the vertical distribution of BrO in the troposphere is largely unknown (Neuman et al., 2010), we have considered two different approaches depending on the surface albedo value:

1. High albedo (>50%): this is the ideal case, with a high sensitivity for BrO close to the surface and a weak dependence of the tropospheric AMF to the shape of the profile (see Fig. 4, brown and black curves). We have made a provisional choice for a tropospheric BrO concentration profile constant in the first km above the Lambertian surface reflector.

2. Low albedo (<50%): as the measurement sensitivity over dark surfaces (such as oceans) is strongly reduced in the boundary layer, we have assumed the tropospheric BrO profile to have only a contribution in the free-troposphere (where the measurement sensitivity is larger by about a factor of five compared to the boundary layer; see Fig. 4). As a result, the retrieved tropospheric BrO columns in such situations are only representative of the free-troposphere, and any BrO amount present in the boundary layer will be largely underestimated. In contrast, the results for high albedo scenes are sensitive to the entire tropospheric vertical column, i.e. free-troposphere and boundary layer. The choice of a free-tropospheric BrO profile constitutes a limitation of our approach; however it is justified by the fact that the typical tropospheric abundances of BrO in the extra-polar boundary layer are either below the detection limit of the satellite instrument or correspond to localized emissions with a spatial extent smaller than the typical pixel size. Our baseline for the retrieval has been to assume a Gaussian profile with a maximum at 6 km high and a full width half maximum of 2 km, consistent with the observed profile of Fitzenberger et al. (2000). The sensitivity of the retrieval to this assumption will be further discussed in Sect. 4.2.

3.4 Error analysis

The total retrieval uncertainty on the tropospheric BrO vertical columns can be derived by error propagation starting from Eq. (1). Considering the different steps of the retrieval algorithm as independent and uncorrelated, the total error on the tropospheric vertical column can be expressed as (Boersma et al., 2004; De Smedt et al., 2008):

$$\sigma^2_{\mathrm{VCD_{tropo}}} = \frac{1}{N}.\left(\frac{\sigma_{\mathrm{SCD_{rand}}}}{\mathrm{AMF_{tropo}}}\right)^2 + \left(\frac{\sigma_{\mathrm{SCD_{syst}}}}{\mathrm{AMF_{tropo}}}\right)^2 + \left(\frac{\sigma_{\mathrm{SCD_{strato}}}}{\mathrm{AMF_{tropo}}}\right)^2 + \left(\frac{(\mathrm{SCD}-\mathrm{SCD_{strato}}).\sigma_{\mathrm{AMF_{tropo}}}}{\mathrm{AMF^2_{tropo}}}\right)^2 \quad (5)$$

where $\mathrm{SCD_{strato}} = VCD_{\mathrm{strato}}.\mathrm{AMF_{strato}}$ denotes the stratospheric BrO slant column.

$\sigma_{\mathrm{SCD_{rand}}}$ and $\sigma_{\mathrm{SCD_{syst}}}$ are the random and systematic parts of the error on the slant columns. The random error is reduced when the number of measurements increases. Therefore, in case of averaging, $\sigma_{\mathrm{SCD_{rand}}}$ can be divided by the square root of the number of satellite pixels taken into the mean (N). $\sigma_{\mathrm{SCD_{strato}}}$ and $\sigma_{\mathrm{AMF_{tropo}}}$ stand for the errors (considered systematic) on the stratospheric slant column and the tropospheric air mass factor, respectively. For each pixel, we have calculated a rough estimate of the random and systematic parts of the error on the tropospheric BrO vertical column. The random slant column error is evaluated for each satellite orbit by the standard deviation of the measured columns around the mean for latitude bands of 5° width. Based on calculations using the formalism of Rodgers (2000) (see also Theys et al., 2007), sensitivity tests made on GOME-2 spectra and the experience with BrO retrieval from GOME and SCIAMACHY (Van Roozendael et al., 2002 and 2004), a typical systematic slant column error of about 20% including the uncertainty on the BrO cross-section and its temperature dependence has been estimated. For the error on the stratospheric slant column, we consider an error equal to 20%, as derived in Theys et al. (2009b). The error on the tropospheric AMF depends on uncertainties on the input parameters (surface albedo, cloud fraction, cloud top height and tropospheric BrO profile shape) and on the sensitivity of the air mass factor to each of them. An estimate of the tropospheric AMF error due to an individual input parameter error is obtained by applying a perturbation method. The total error on the tropospheric AMF is then calculated from the sum of squares of the contributions to the tropospheric AMF error due to errors on the individual input parameters. The latter input parameter absolute uncertainties are taken as follows (Koelemeijer et al., 2002 and 2003): surface albedo error: 0.02, cloud fraction error: 0.05 and cloud

top height error: 1 km. The error on the profile shape is estimated considering a 2 km uncertainty on the bulk altitude of the BrO profile.

4 Verification of the retrievals

In this section, the reliability of the GOME-2 BrO columns is assessed through comparisons with SCIAMACHY satellite nadir observations (total BrO columns) and independent ground-based observations (stratospheric and tropospheric BrO columns).

4.1 Comparison to SCIAMACHY nadir observations

SCIAMACHY is in operation on the ENVISAT platform since July 2002. The instrument flies on polar sun-synchronous orbits and crosses the equator 30 minutes after GOME-2 (at 10:00 LT). The instrument observes the Earth's atmosphere in limb, nadir and occultation viewing geometries. The measurements are performed in eight channels covering the 240–2380 nm wavelength range with a spectral resolution of 0.2 to 1.5 nm. A detailed description of SCIAMACHY can be found in Bovensmann et al. (1999). In this study, we use the nadir BrO total columns derived at the Institute of Environmental Physics (IUP) of the University of Bremen. A description of the retrieval algorithm can be found in Afe et al. (2004). However, the most recent retrieval version differs slightly in the retrieval settings. The spectral analysis is performed in the 336–351 nm interval (instead of the less stable 336–347 nm interval in Afe et al., 2004) and includes the absorption of BrO (243 K), O_3 (223 K and 243 K), NO_2 (223 K), O_4 as well as two Ring pseudo-spectra for correction of the effect of Rotational Raman scattering and a polynomial of order 4. To account for long-term drifts in the SCIAMACHY data, all slant columns are normalised to the daily value observed over the equatorial Pacific (150° E–270° E longitude, 10° S to 10° N latitude) assuming a constant vertical column of 3.5×10^{13} molec cm^{-2}. A similar correction has previously been applied to GOME BrO measurements (Richter et al., 2002) While this improves the overall consistency of the SCIAMACHY BrO data set, it also removes any real seasonal or interanual variability in the data over the equator. For our comparison exercise, we have calculated averaged total BrO columns from SCIAMACHY and GOME-2 observations (SZA$<$80°) for six latitudinal bands (60–90° S, 30–60° S, 0–30° S, 0–30° N, 30–60° N, 60–90° N), for each day in 2007 and 2008. For this purpose, we have applied simple geometrical air mass factors (i.e., AMF = sec(θ_0) + sec(θ) where θ_0 and $\theta$are the solar and viewing zenith angles, respectively) to the retrieved slant columns of both instruments. Figure 5 shows the comparison results. The agreement between GOME-2 and SCIAMACHY BrO columns is generally good; the seasonality of BrO being consistently captured at all latitudes by both satellite data. The differences between SCIAMACHY and GOME-2 total columns are most of the time lower than $\pm 0.5 \times 10^{13}$ molec cm^{-2}. Considering the systematic uncertainties on satellite measurements typically of the order of 1×10^{13} molec cm^{-2}, the observed differences are within the error bars.

4.2 Comparison to ground-based observations

Ground-based UV-visible zenith-sky observations of BrO have been performed at Harestua (60° N, 11° E; operated by IASB-BIRA) and Lauder (45° S, 170° E; operated by NIWA). Both stations belong to the Network for the Detection of Atmospheric Composition Change (NDACC) and are remote sites not influenced by local pollution sources. Measured radiance spectra are analysed for differential BrO slant column densities using the DOAS technique. The profiling algorithm described and extensively used in Hendrick et al. (2007, 2008 and 2009) is then applied to the ground-based BrO slant column densities in order to retrieve BrO vertical profiles. Stratospheric and tropospheric BrO columns are calculated by integrating the retrieved profiles in the appropriate altitude ranges. As the retrieved ground-based BrO profiles are representative of the situation at twilight, a photochemical correction is applied in order to match the solar zenith angle corresponding to the satellite overpass time. Figure 6 shows the comparison between the ground-based and the coincident GOME-2 stratospheric (climatology) and tropospheric BrO columns for the period 2007–2008, at Harestua. Daily mean GOME-2 BrO column amounts are calculated based on the full retrieval technique described in Sect. 3 and using all pixels (that are not rejected by the cloud selection criteria) with a solar zenith angle lower than 80° and falling within a radius of 200 km around Harestua. In general, climatological BrO stratospheric vertical columns are found to be in good agreement with the stratospheric columns inferred from the ground-based observations, in terms of mean level and seasonal variation (with a tendency to produce lower values by 0.15 ± 0.5 10^{13} molec cm^{-2} on average). Note that even short-term variations of the stratospheric column are well captured by both datasets, especially in spring. Figure 6 also indicates that both satellite and ground-based observations are consistent with a tropospheric BrO column of 1.5×10^{13} molec cm^{-2}. Note that the GOME-2 tropospheric BrO columns are weakly dependent on the bulk altitude of the tropospheric BrO profile assumed in the retrieval (6 km or 8 km, blue and black lines, respectively).

Using the same settings, Fig. 7 shows the comparison between GOME-2 and ground-based stratospheric and tropospheric BrO columns at Lauder, for the period September 2007–October 2008. The agreement between GOME-2 and ground-based data is generally good for the stratospheric columns. For Southern hemisphere winter time, the stratospheric climatology has however a tendency to produce

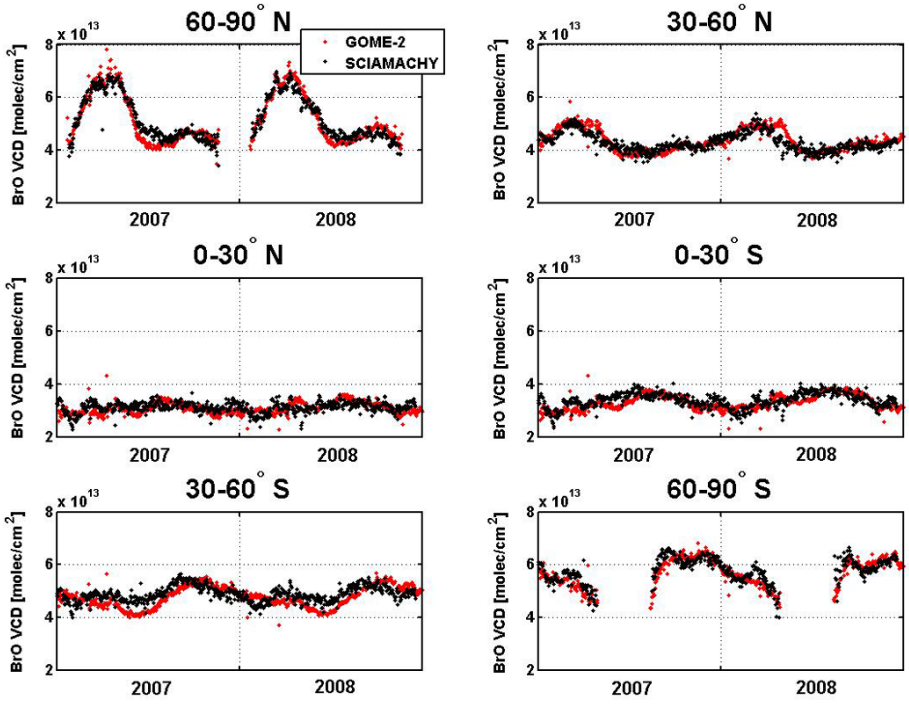

Fig. 5. Time-series of total BrO vertical columns from GOME-2 and SCIAMACHY nadir observations for different latitudinal bands (daily zonal averages). Only data corresponding to solar zenith angles lower than 80° are shown.

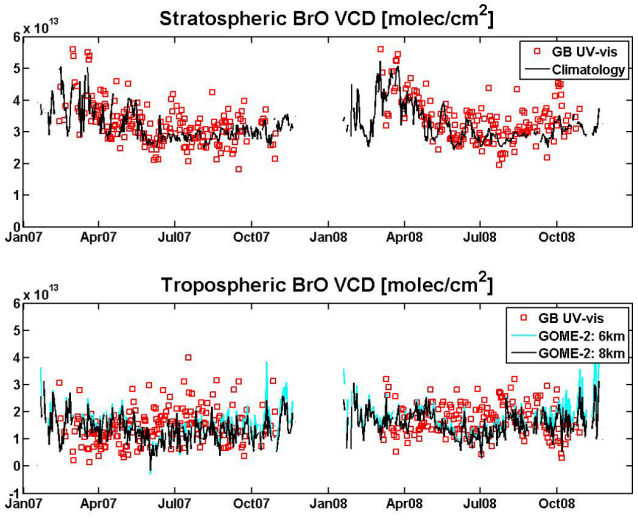

Fig. 6. Comparison between GOME-2 and ground-based stratospheric (upper plot) and tropospheric (lower plot) BrO vertical columns, at Harestua for the period 2007–2008. Two assumptions are made in the GOME-2 retrieval algorithm for the height (6 km: blue line, 8 km: black line) of the maximum tropospheric BrO concentration (see text).

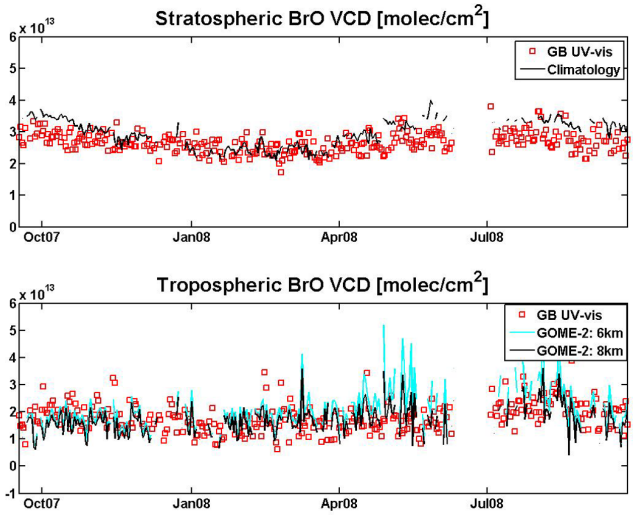

Fig. 7. Same as Fig. 6, at Lauder for the period September 2007–October 2008.

slightly higher values than the ground-based data (by $\sim 0.5 \times 10^{13}$ molec/cm^2). The agreement between GOME-2 and ground-based tropospheric columns is generally also good, except from mid-April to end August 2008 where the GOME-2 tropospheric BrO columns (blue line) are systematically higher than the values retrieved from the ground-based observations (mean bias: 0.7×10^{13} molec/cm^2). It should be noted that the winter period at Lauder corresponds to conditions of high SZA and low surface albedo (not encountered at Harestua), making the weighting functions critically

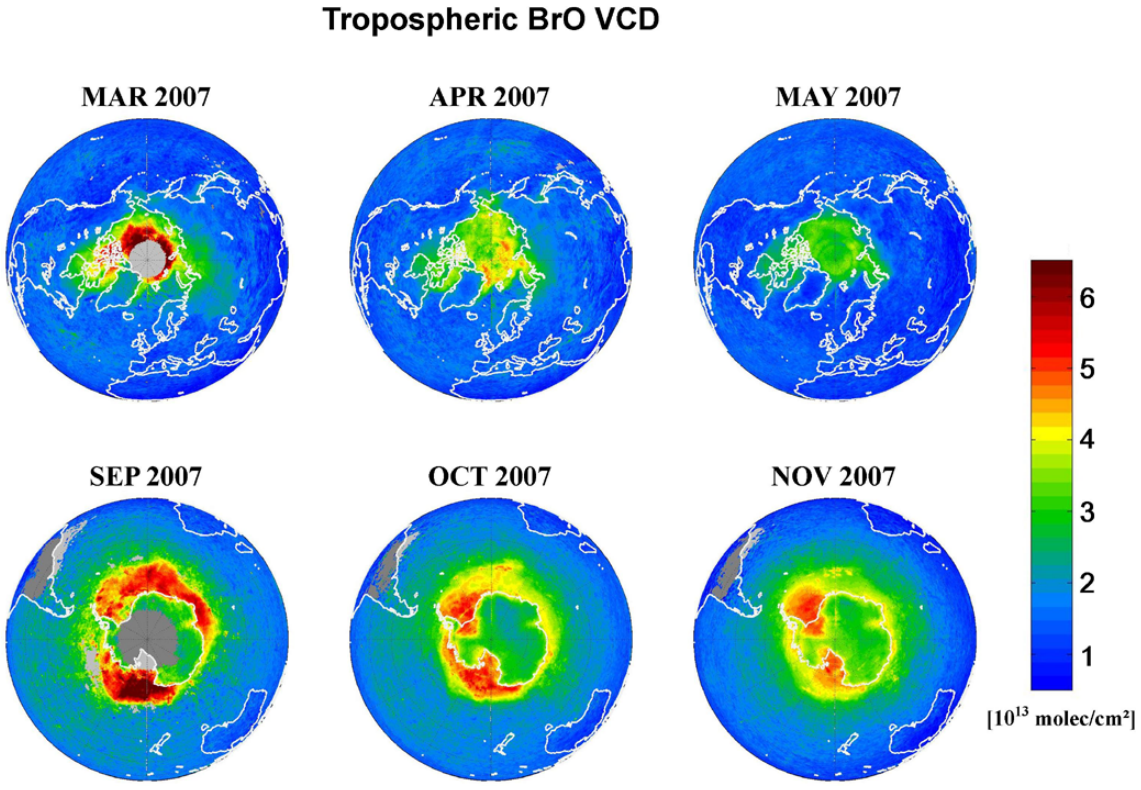

Fig. 8. Monthly averages of GOME-2 tropospheric BrO vertical columns in polar spring 2007 for the Northern Hemisphere (upper plots) and the Southern Hemisphere (lower plots). Only data corresponding to solar zenith angles lower than 80° are used.

dependent on the altitude in the troposphere and therefore yielding a rather uncertain stratosphere-troposphere BrO separation. If one assumes a tropospheric BrO profile shape peaking at 8 km (black lines in Fig. 7) rather than 6 km (as it is routinely used in our standard retrieval), the agreement between satellite and ground-based data significantly improves (with GOME-2 being lower than the ground-based data by 0.13 ± 0.7 10^{13} molec cm^{-2} on average). Note however that this is not a firm proof for BrO being higher up. One can say that given the uncertainties on the tropospheric air mass factor at Lauder, ground-based and GOME-2 BrO observations agree reasonably well.

From Figs. 6 and 7, we conclude that both ground-based and satellite observations are consistent with a tropospheric BrO column of $\sim 1.5 \times 10^{13}$ molec cm^{-2} for morning conditions ($\sim$09:30 solar local time), although the errors on the tropospheric BrO columns are rather large: typically around 0.5×10^{13} molec cm^{-2} for the ground-based data and about 0.8–1.5×10^{13} molec cm^{-2} for the satellite observations.

5 Results and discussion

Using the retrieval scheme described in Sect. 3, tropospheric BrO columns have been computed for GOME-2 measurements taken in 2007 and 2008. As an example, Fig. 8 displays the spatial distribution of the monthly averaged tropospheric BrO columns from GOME-2 for the polar spring period 2007 in both hemispheres (analogous results are obtained for the year 2008). The areas left in grey correspond to zones with no satellite overpass, solar zenith angles larger than 80° or regions strongly affected by the South Atlantic Anomaly in the earth geomagnetic field (over South America). In Fig. 8, large BrO columns are observed during polar spring in both hemispheres. These events are related to polar tropospheric BrO precursors emissions and have already been highlighted in previous studies (Wagner and Platt, 1998; Richter et al., 1998, 2002; Chance, 1998). The regions with enhanced tropospheric BrO columns exhibit an excellent correlation with the areas of sea ice. The difference in BrO distribution between both hemispheres mainly reflects the differences in sea-ice distribution.

5.1 Stratospheric BrO

We first concentrate on demonstrating the suitability of the stratospheric BrO climatology used in this work (Sect. 3.2), in particular its ability to reproduce the observed spatial structures of stratospheric BrO, and to correct for them. As an illustration, Fig. 9 presents a comparison between GOME-2 total BrO columns (estimated using stratospheric AMFs, no cloud filtering) and the corresponding stratospheric BrO

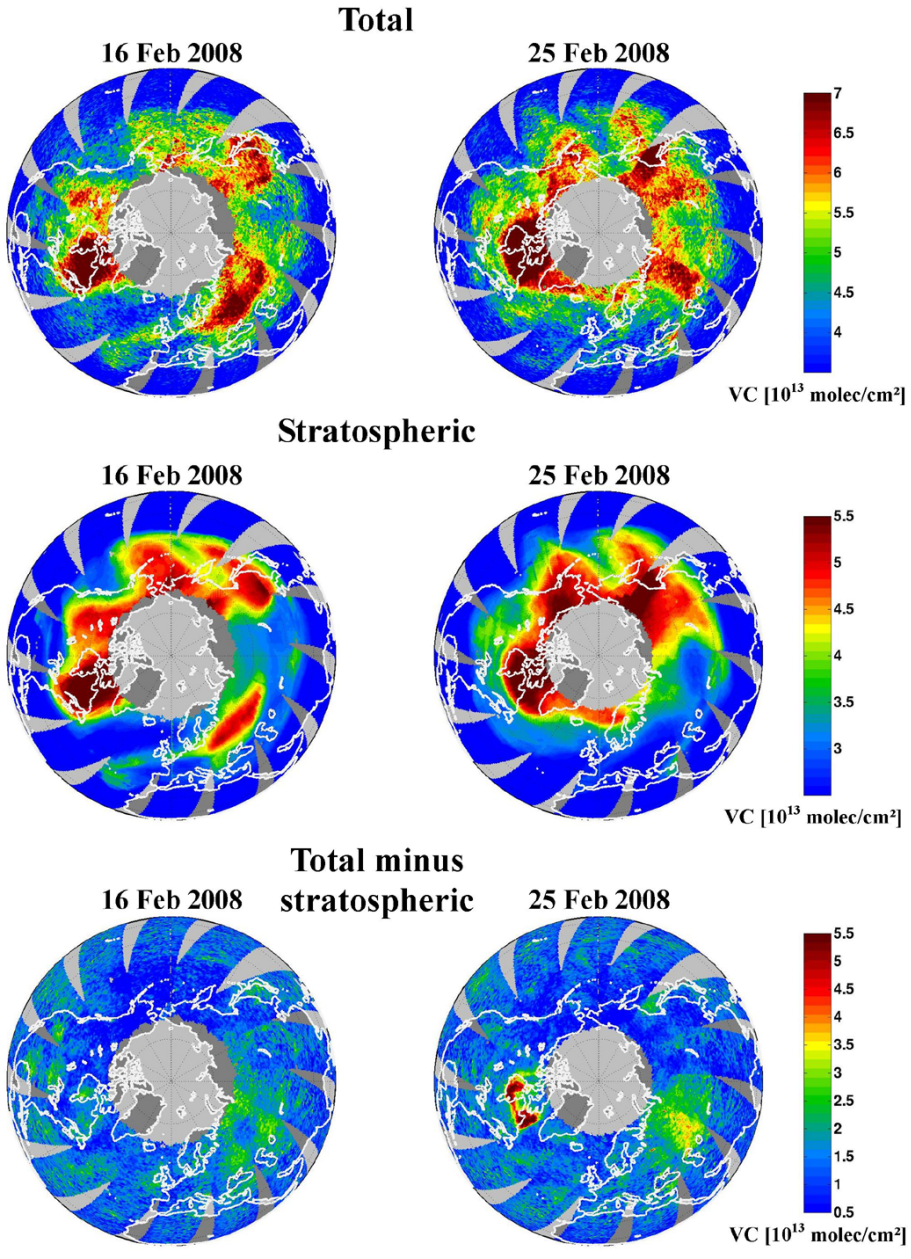

Fig. 9. GOME-2 total BrO columns (upper plots), stratospheric BrO columns calculated from the BASCOE climatology at GOME-2 overpass (center plots) and the difference between the total and stratospheric BrO columns (lower plots). Total BrO columns are estimated using stratospheric air mass factors. The results are presented for the (left) 16 and (right) 25 February 2008. Note that the color scale of the total column maps has been chosen in a way that the correlation with stratospheric BrO structures can be best visualized, although it is not optimal to represent the large range of total BrO column values.

vertical columns derived from our climatology, for two days in February 2008 in the Northern Hemisphere. The data of 16 February 2008 (left plots) have been selected because large-scale dynamical structures of stratospheric origin are observed in the measured total BrO map and at the same time the influence of tropospheric BrO on the measurements is moderate (absence of large and persistent plumes of tropospheric BrO). One can see that the stratospheric BrO climatology qualitatively reproduces very well the dynamical structures of stratospheric BrO observed by the satellite. This is further confirmed when examining the map of the difference between the total and stratospheric columns. No evidence of remaining structures can be found beyond the range of observed background values. The data of 25 February 2008 in Fig. 9 (right plots) reflect another typical situation: in addition to the large-scale stratospheric BrO structures

(consistently reproduced by the climatology), patterns of elevated tropospheric BrO columns are also observed in the vicinity of the Hudson Bay and the Caspian Sea. These structures show only little correlation with the simulated stratospheric BrO field and therefore can not be explained by a mismatch in the stratospheric BrO correction. The results of Fig. 9 are important not only because they consolidate our inversion approach, but also because they allow to address new issues, some of them already raised in previous papers: (1) the free tropospheric BrO background at mid-latitudes might be at least partly caused by transport of BrO enriched air masses from the polar boundary layer (Hollwedel, 2005), (2) a number of elevated total BrO columns observed from satellite instruments during Arctic spring can have stratospheric origin (Salawitch et al., 2010). Clearly such topics can only be studied properly by separating the stratospheric and tropospheric BrO structures in the total BrO column field measured from space.

Figure 10 presents an illustration of events typically observed in the Arctic spring. Total, stratospheric and tropospheric BrO columns measured in the Northern Hemisphere are represented over a period of three days in April 2008. Also shown are the corresponding tropopause heights. In this case, the full inversion scheme described in Sect. 3 has been used to determine the tropospheric and stratospheric BrO columns. Several features can be observed. First, the stratospheric BrO columns anti-correlate with the tropopause height field, the largest stratospheric BrO columns being found (as expected) at low tropopause height. Secondly, some of the total BrO column hotspots seen by GOME-2 exhibit spatial patterns similar to model estimates of stratospheric BrO column. These results are consistent with those reported by Salawitch et al. (2010). However, there are also regions of enhanced total BrO columns that are located in areas with low stratospheric BrO. We attribute this enhancement unambiguously to tropospheric BrO. Finally, a closer look to the BrO column results shows that several BrO hotspots are observed in both stratospheric and tropospheric fields. In the following, we investigate several explanations for this behaviour.

Although our stratospheric correction accounts for changes in tropopause heights (through its ozone column dependence), the stratospheric BrO columns may occasionally deviate from the climatological values for special conditions (e.g., extremely low tropopauses typically down to 5-6 km height). In such cases, a possible underestimation of the stratospheric BrO column results, leading to an overestimation of the tropospheric BrO columns, cannot be excluded. We have estimated this effect by calculating an upper limit of the difference between the stratospheric BrO columns from the climatology and from the BASCOE model run used to generate the climatological dataset (Theys et al., 2009b), for the conditions of BrO enriched descending air. When considering also the BrO column amount possibly transported below the tropopause by an intrusion of stratospheric air in the troposphere, one estimates errors in the range of 1×10^{13} molec cm^{-2}. By inspecting the results of Fig. 10 over the Hudson Bay region (55–70° N, 70–96° W) in conditions of very low tropopause heights, one can see that the retrieved tropospheric BrO columns in some instances do not exceed the surrounding tropospheric BrO background by more than this limit. This means that for these particular conditions, we cannot fully exclude that the enhancement of total BrO amount measured might be of stratospheric origin (either explained by a mismatch in the stratospheric BrO correction or by a stratospheric BrO intrusion). This is in line with the interpretation of the satellite total column BrO given by Salawitch et al. (2010). We have investigated the frequency of occurrence of such features for the spring season over the Hudson Bay area (55–70° N, 70-96°W) and for the Northern high latitudes (55–90° N) in general. For this purpose, we have considered in our analysis only the satellite "BrO hotspots", defined as the regions where total column BrO is elevated by at least 2×10^{13} molec cm^{-2} relative to the zonal mean (Salawitch et al., 2010). We have also defined a criterion to select the "events of possible stratospheric origin" among these measurements. The latter criterion is based on the retrieved residual BrO vertical columns. We consider that if the retrieved value is lower than a certain threshold then it is difficult to conclude whether there is an enhanced amount of BrO in the troposphere, and therefore a stratospheric event is a possible explanation. The limit chosen is 3.5×10^{13} molec cm^{-2}. This value is equal to the averaged tropospheric BrO column ($\sim 2.5 \times 10^{13}$ molec/cm^2) for the observations where a stratospheric event is unlikely (ozone columns < 350 DU) plus the uncertainty on the stratospheric correction of 1×10^{13} molec cm^{-2} (already introduced above). The results are displayed in Fig. 11, where we show the histograms of the retrieved tropospheric BrO vertical columns for the Northern high-latitudes and over the Hudson Bay. The data are from February to May (2007 and 2008); the tropospheric column threshold of 3.5×10^{13} molec cm^{-2} is also shown (brown dashed-line). The black and red curves correspond to the frequency distributions for O_3 columns lower or larger than 450 DU, respectively, while the blue lines represent all measurements. From Fig. 11, it is clear that a stratospheric event can only be observed for sufficiently large O_3 columns. This is what we expect as high ozone column is a prerequisite for a stratospheric BrO intrusion. Based on Fig. 11, one can also say that the stratospheric events are not very frequent for the Northern high-latitudes; the percentage of observations with tropospheric BrO columns lower than the threshold (brown dashed-line) is about 10% for ozone columns larger than 450 DU and 3% in general. However, this behaviour is more frequent over the Hudson Bay region where the frequency is 20% for ozone columns larger than 450 DU and 10% if no distinction based on ozone column is made.

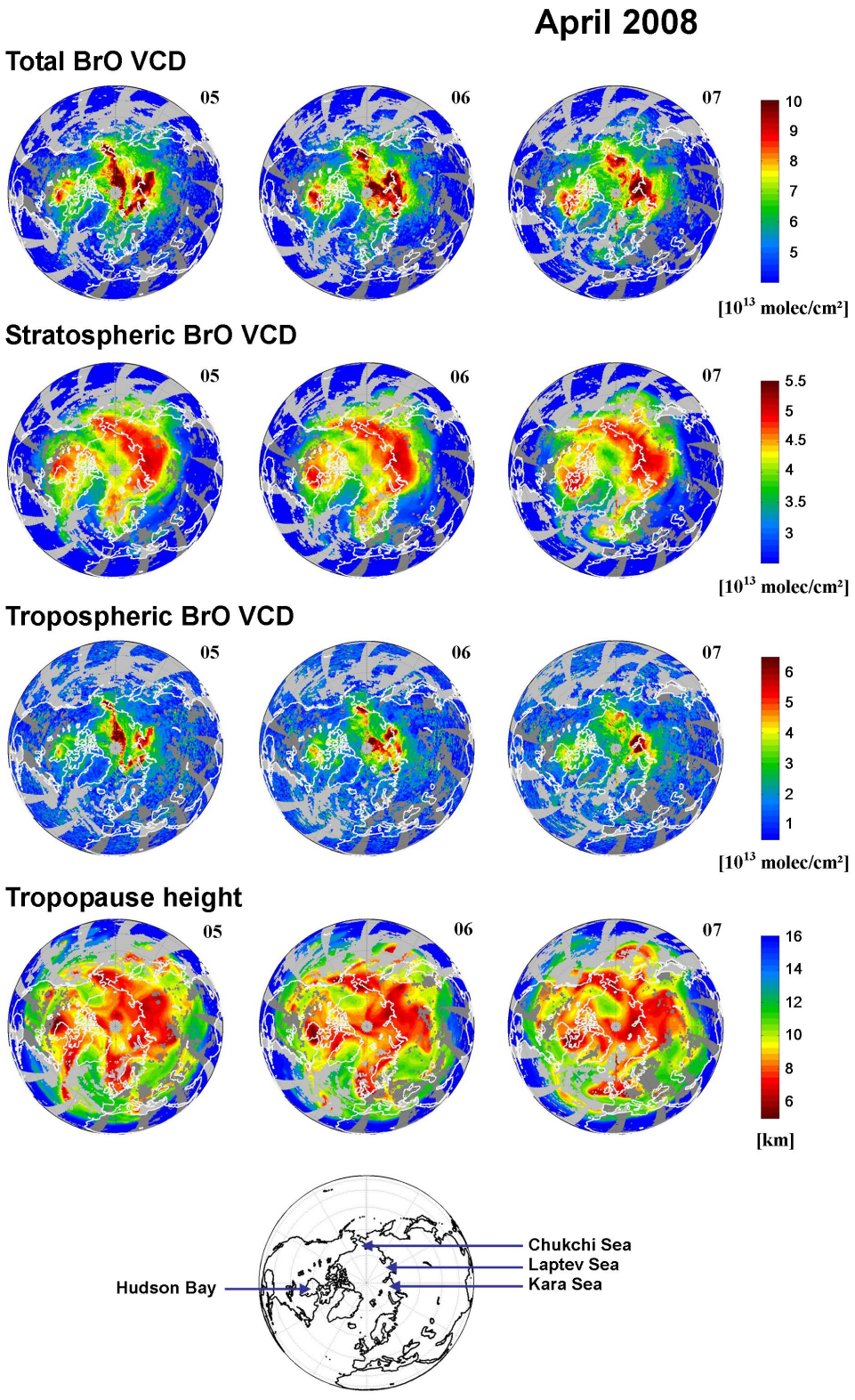

Fig. 10. GOME-2 BrO columns (total, stratospheric and tropospheric) and tropopause height (from ECMWF data). The results are presented for selected days in April 2008 (5 to 7 April, from left to right) in the Northern Hemisphere. The regions contaminated by clouds have been left in grey.

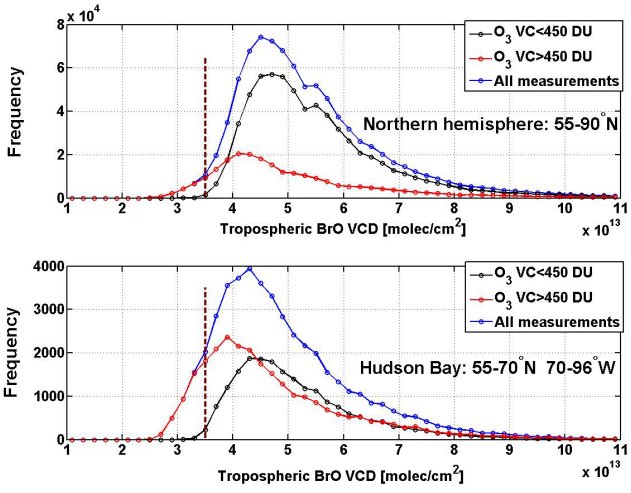

Fig. 11. Histograms of GOME-2 tropospheric BrO vertical columns for the satellite "BrO hostpots" observations (regions where BrO total columns are elevated by at least 2×10^{13} molec cm^{-2} relative to the zonal mean). The data from February to May (2007 and 2008) are considered for (upper plot) the Northern Hemisphere (55–90° N) and (lower plot) the Hudson Bay (55–70° N, 70–96°W). Black and red lines show the frequency distributions of data with O_3 vertical columns lower and higher than 450 Dobson Units, respectively. Blue lines: no distinction is made. The brown vertical dashed line corresponds to the upper limit of the residual tropospheric BrO vertical columns for the events of possible of stratospheric origin (see text).

It should be noted that all these percentage values represent upper limits of the frequency of stratospheric events, since they also include weak or localized tropospheric BrO events.

5.2 Polar tropospheric BrO

Let us examine the results of Fig. 10 for low tropopause heights in regions like the Laptev and Kara Seas (north of the Siberian coasts) and the Chukchi Sea (close to the Bering Strait). It can be seen that some (but not all) low tropopause areas in theses regions are collocated with tropospheric BrO hotspots. However, the residual columns of these tropospheric BrO hotspots are too high to be explained solely by a stratospheric effect (according to the above discussion). Therefore, it is likely that these tropospheric BrO hotspots are related to BrO precursors emissions at the surface.

We have further investigated the link between low tropopause heights and elevated tropospheric BrO columns (already discussed in Begoin et al., 2010). Figure 12 (upper plots) shows the frequency distribution of the results as a function of the tropopause height (for different values of tropospheric BrO vertical columns), for the 2007–2008 period in both Arctic and Antarctic regions. One can see that the distribution of data is clearly shifted towards low tropopause heights when the tropospheric BrO vertical columns increase, albeit large tropospheric BrO events are frequently observed under conditions of high tropopause. Sensitivity tests have been carried out in order to estimate the impact of a stratospheric BrO column error of ±20% on the retrieved tropospheric columns. This leads only to a slight change of the frequency distribution of the results displayed in Fig. 12. This effect appears as a common behaviour in polar spring, although it seems to be more important in the Arctic than in the Antarctic region. We speculate that this feature might be connected to a relation between the tropopause height (linked to weather systems) and essential variables for BrO generation in the polar troposphere (e.g., temperature, illumination, availability of surfaces for heterogeneous reactions, etc.). One possible explanation could be a dynamically driven bromine emission mechanism: low tropopause is frequently associated to low pressure cyclone systems and strong surface winds. Recent studies (Yang et al., 2008 and 2010; Jones et al., 2009 and 2010) have provided convincing indications that the production of sea salt aerosol from snow lying on sea ice during blowing snow events (triggered by very strong surface winds) and the subsequent release of bromine, could be an important contribution to the bromine explosion phenomenon in the polar regions (Arctic and Antarctic). In order to investigate whether our analysis reflects this process assumed for bromine explosions, we have compared results of Fig. 12 to simulations from the *p*-TOMCAT model. *p*-TOMCAT (parallel-Tropospheric Off-Line Model of Chemistry and Transport) is an off-line three-dimensional tropospheric chemical transport model with a detailed bromine chemistry scheme that contains gas-phase reactions and heterogeneous reactions on cloud particles and aerosols, as well as bromine removal from dry and wet deposition (Yang et al., 2005, 2008 and 2010). It includes bromine emissions from sea salt, bromocarbon photo-oxidation and also a parameterization for sea salt aerosol production through blowing snow events (in the latest version of *p*-TOMCAT; see Yang et al., 2010). For the present study, the model was run for the 2007-2008 period at a horizontal resolution of 2.8° × 2.8° and an output frequency of 2 h using winds and temperature derived from the ECMWF operational analysis. For each grid box, we have calculated a daily maximum tropospheric BrO column based on the modelled BrO profiles and a corresponding dynamical tropopause height (using the definition of the dynamical tropopause in Sect. 3.2). Using this modelling data set, we have done the same statistical analysis as for GOME-2 data; the results are presented in Fig. 12 (lower plots). One can clearly identify similarities in both hemispheres between the modelling and the retrieved results for the distribution of the tropospheric BrO columns as a function of the tropopause height. The general tendency of elevated tropospheric BrO columns linked to low tropopause heights being well captured by the *p*-TOMCAT model. It should be noted that the model definitely fails to reproduce the observed features when the blowing snow-sourced bromine is omitted (in line

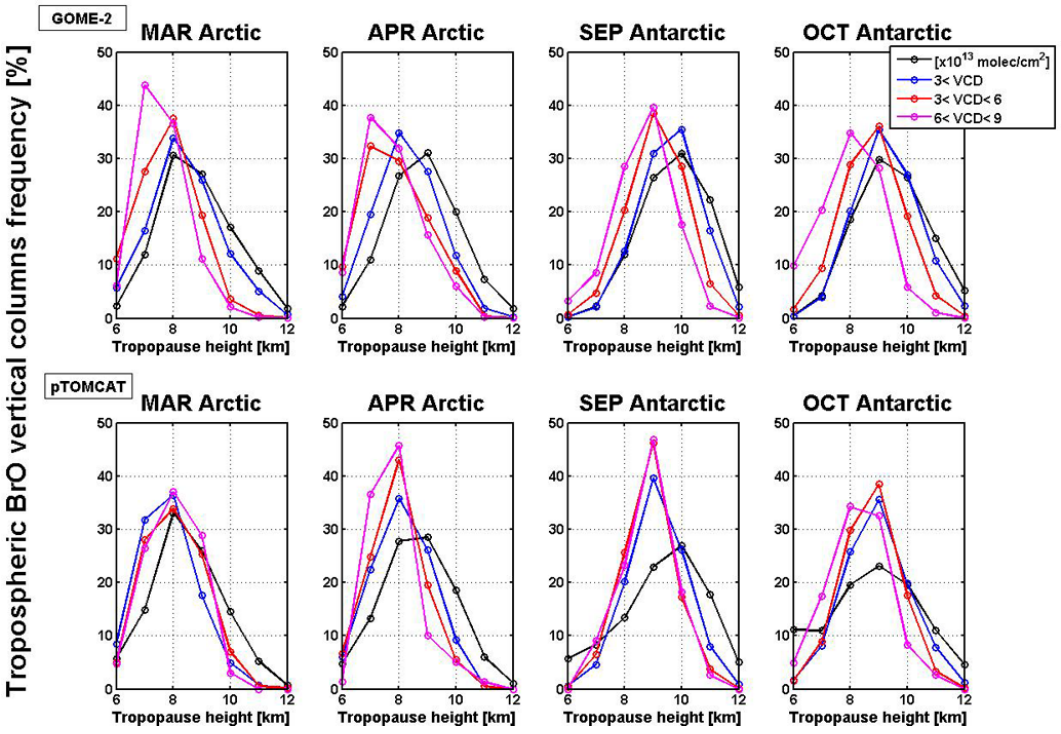

Fig. 12. Frequency distribution (expressed in %) of the GOME-2 (upper row) and *p*-TOMCAT (lower row) tropospheric BrO vertical columns as a function of the altitude of the tropopause (±0.5 km), for different ranges of vertical columns. The results are shown separately for different months in spring in the Northern Hemisphere (55–90° N; March and April) and Southern hemisphere (55–75° S; September and October). Only data corresponding to solar zenith angles lower than 80° are considered here.

with the findings of Yang et al., 2010). The results of Fig. 12 provide an indication that the release of bromine by blowing snow events might play a role in the bromine explosion phenomenon, in both the Arctic and Antarctic. However, one should be cautious with this interpretation since other dynamically driven bromine production mechanisms may possibly lead to similar behaviour. It is also worth adding that in another recent study, Begoin et al. (2010) have used GOME-2 data to study an event of long range transport of BrO plume in the Arctic lower troposphere in spring 2007. Using trajectory calculations, they found quite similar dynamics in the troposphere and lower stratosphere for this particular event. In particular the BrO hotspot of interest was clearly linked to the low tropopause heights. If this transport-related feature is frequent in the polar region, it can reinforce (and also complicate) the relation between low tropopause heights and high tropospheric BrO columns, as displayed in Fig. 12.

In order to further investigate the relevance of the blowing-snow mechanism, we present two examples of events (Fig. 13) found in the GOME-2 tropospheric BrO vertical column maps that are directly reproduced by the *p*-TOMCAT simulations (interpolated to the time and location of GOME-2 overpass). It shows clearly the generation of BrO plumes in the polar boundary layer over the Chukchi Sea (3–5 April 2008, Arctic) and the Ross Sea (22–24 October 2007, Antarctic). Noteworthy is the good coincidence in magnitude, space and time between GOME-2 and *p*-TOMCAT tropospheric BrO plumes. Both events are associated to strong surface winds and can only be explained by including the blowing snow mechanism in the *p*-TOMCAT model. Both BrO plumes are confined in the polar boundary layer (below 1.5 km height) with BrO mixing ratios as high as 30 pptv. Although the results of Fig. 13 can be reasonably well explained by the mechanism of bromine release from blowing snow events, they provide no indication on the precise magnitude of this blowing snow source compared to other processes. It should also be emphasized that beyond the cases displayed in Fig. 13, there are also large discrepancies between the model and the measurements. This is either due to the fact that the *p*-TOMCAT Br emission is highly parameterized (the limiting uncertainties coming from the snow salinity and the fraction of bromine in sea salt aerosol which is released in gaseous form into the atmosphere – the bromine depletion factor; see Yang et al., 2010) and/or that other possible bromine sources are missing in the model.

Nevertheless, the results presented here call for further modelling developments supported by satellite BrO measurements and in-situ measurements during blowing snow events in order to better assess the relative contributions of bromine sources in the polar troposphere. Though it goes far beyond

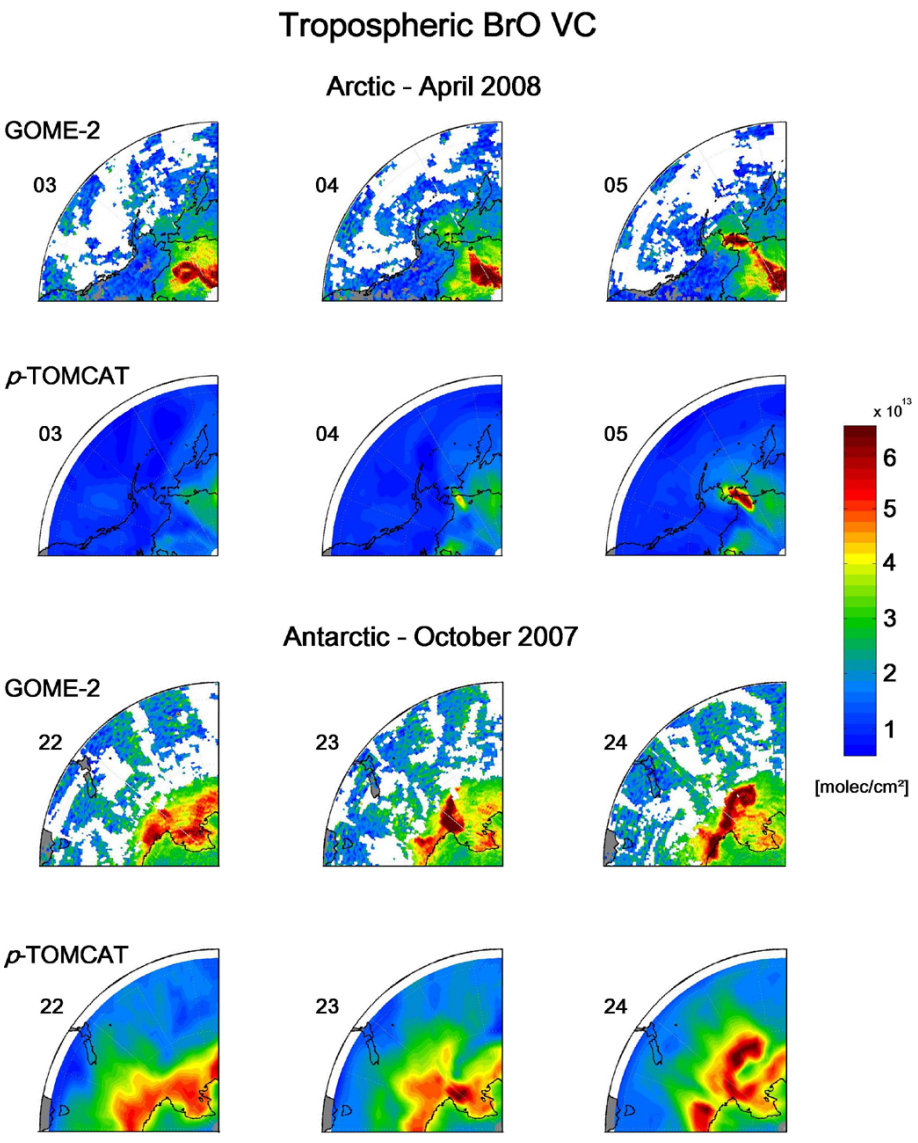

Fig. 13. Tropospheric BrO vertical columns from GOME-2 and *p*-TOMCAT across the Chukchi Sea region of Arctic from 3 to 5 April 2008 (upper panels) and over the Ross Sea of Antarctica from 22 to 24 October 2007 (lower panels).

the scope of this paper, this is of great importance especially to better assess future tropospheric bromine emissions in response to climate change (Arctic warming, increase of first year sea ice coverage and increase of anthropogenic emissions, e.g. from shipping).

5.3 Extra-polar tropospheric BrO

Turning to global fields, we now investigate the latitudinal and seasonal variations of the retrieved tropospheric BrO vertical columns. For this purpose, monthly averages of tropospheric BrO columns have been computed for different latitudinal bands in both hemispheres. The results are presented in Fig. 14, together with estimates of the corresponding retrieval errors that include all sources of uncertainties (details are given in Sect. 3.4). We have also plotted the variability of the data (1σ) within each latitudinal band and month. It is important to note the large variability of the resulting tropospheric vertical columns. Although a fraction of this variability originates from the natural variability of tropospheric BrO (e.g. during spring at high latitudes), an important part of the observed variations results from the propagation of the instrumental noise through the DOAS analysis. When averaging (as in Fig. 14), the random error is largely reduced and the total error on the averaged tropospheric BrO vertical columns is dominated by systematic errors. The latter errors (grey-dashed area) are estimated to be in the range from 1×10^{13} molec cm^{-2} in summer to 1.5–2 $\times 10^{13}$ molec cm^{-2} in winter. From Fig. 14, it can be

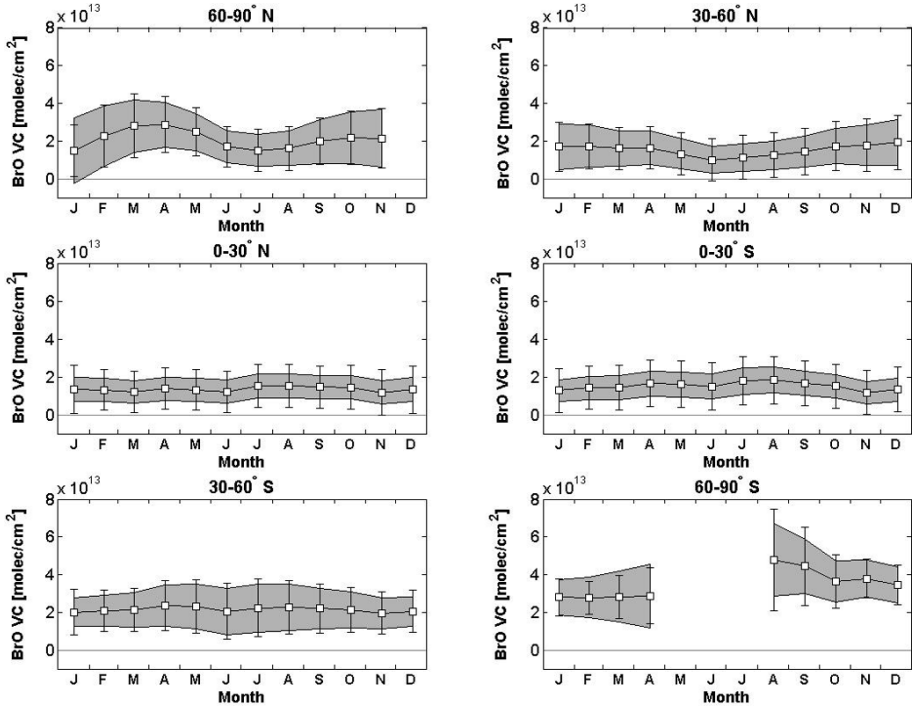

Fig. 14. Zonal mean of tropospheric BrO vertical columns as a function of time (monthly averages). The grey-dashed area indicates the total error on the tropospheric BrO vertical columns (see text). The error bars correspond to 1-sigma standard deviation of the data around the mean. The data used are from 2007 to 2008, and solar zenith angles lower than 80°.

stated that, except for the results at high latitudes in spring, the seasonal and latitudinal variations of the tropospheric BrO columns are generally rather small, with a magnitude lying within the uncertainties of the retrieved tropospheric BrO columns. Our analysis tends to confirm the findings of other studies (Fitzenberger et al., 2000; Wagner et al., 2001; Richter et al., 2002; Van Roozendael et al., 2002; Hendrick et al., 2007; Theys et al., 2007) that a tropospheric BrO background with vertical columns of 1–3 $\times 10^{13}$ molec cm^{-2}, in addition to the polar BrO emissions occurring in spring, must be present at the global scale for all seasons. This is in contrast to three studies using spectral observations of direct-sun geometry, at Lauder (Schofield et al., 2004), Arrival Heights, Antarctica (Schofield et al., 2006) and in the tropics (Dorf et al., 2008) showing tropospheric columns significantly less i.e. 0.2–0.3 $\times 10^{13}$ molec cm^{-2} and tropospheric BrO mixing ratios lower than 1 pptv, respectively, indicating that more study is required on this subject.

We have further tested the assumption of a significant tropospheric BrO background by making use of GOME-2 cloudy pixels, with the aim to obtain an independent estimate of the BrO content in the troposphere. The approach is similar in concept to the one used to derive tropospheric ozone from the TOMS satellite instrument ("Cloud slicing"; Ziemke et al., 2001). This technique takes benefit of the opaque property of clouds to UV radiation and the enhanced measurement sensitivity above the cloud-top (see Fig. 4, purple curve). As the measurement sensitivity vanishes below the cloud, larger tropospheric BrO slant columns should be measured for lower clouds, if a substantial amount of BrO is present in the troposphere. This is precisely what is observed in Fig. 15 which shows the correlation between tropospheric BrO slant columns (cloud fractions>70%) from GOME-2 measurements (taken in December as an example) and the collocated cloud top pressure (from FRESCO+). In order to scan vertically an important portion of the troposphere, we have selected the data over the tropical latitude band (30° S–30° N). This is justified by the fact that some clouds associated to convective processes can reach much higher altitudes in the tropical region than at other latitudes. In Fig. 15, tropospheric BrO slant columns range roughly from zero at 200 hPa to about 5×10^{13} molec cm^{-2} at ground level (1000 hPa). One can see that most of the BrO (>75%) is present in the atmospheric layers above 700 hPa, i.e. in the free-troposphere. Considering the BrO slant column increment of 5×10^{13} molec cm^{-2} in the tropical troposphere, it is possible to calculate an average tropospheric vertical column by applying an effective above-cloud tropospheric AMF (AMF ~3–3.5, according to Fig. 4). This leads to a tropospheric BrO vertical column of about 1.5×10^{13} molec cm^{-2}, which is in reasonable agreement with the estimated values for the tropospheric BrO background vertical column obtained throughout this work (Figs. 6, 7 and 14) and the BrO column

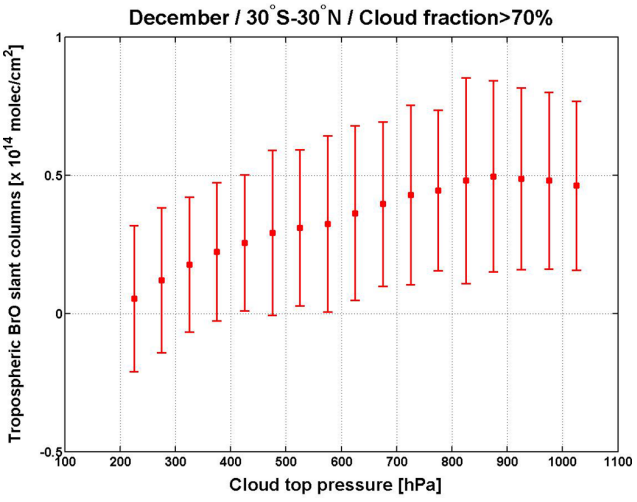

Fig. 15. GOME-2 tropospheric BrO slant columns as a function of cloud top pressure (cloud fraction>70%), in December for $-30° \leq$ latitude $\leq 30°$. The red squares correspond to the mean tropospheric BrO SCD values for cloud top pressure bins of 50 hPa, and the error bars represent the variability of the column within each bin (1σ).

amount of about $1.1 \pm 0.45 \times 10^{13}$ molec cm^{-2} inferred from ground-based multi-axis DOAS measurements in Reunion Island (Theys et al., 2007). It should be noted that similar results were reported by Richter et al. (2002) based on an analysis of the correlation between BrO and O_4 slant columns from the GOME instrument.

6 Conclusions

We have developed an algorithm to retrieve tropospheric BrO columns from satellite nadir UV/visible radiance measurements. The tropospheric columns are derived from a residual technique that combines measured DOAS slant columns and calculated stratospheric columns, and that accounts for the impact of clouds, surface reflectivity and viewing geometry on the measurement sensitivity. The stratospheric BrO correction makes use of a recently developed dynamical climatology of stratospheric BrO (Theys et al., 2009b). This climatology has been generated using BrO profiles from the BASCOE three-dimensional chemical transport model, which includes a contribution of 6 pptv to the stratospheric Br_y budget from short-lived brominated sources gases. Moreover, model simulations have been extensively validated through comparison with several independent correlative data sets of stratospheric BrO observations.

We have successfully applied this algorithm to two years (2007–2008) of data from the GOME-2 instrument, analyzed using improved DOAS settings. The consistency between our BrO retrieval and correlative data has been verified and a good agreement has been obtained with SCIAMACHY nadir observations and ground-based zenith-sky observations. We have demonstrated that our method enables to separate the stratospheric and tropospheric BrO structures in the total BrO column field measured from space. Hence it results in a refined and more quantitative interpretation of the nadir BrO observations. In line with the findings of Salawitch et al. (2010), we found that elevated total column BrO observations in polar spring can occasionally be explained by an increase in stratospheric BrO column due to tropopause descend, and a possible stratospheric intrusion of BrO into the free-troposphere. However, the strong polar BrO hotspots observed, which, interestingly, are often associated to low tropopause heights, cannot be explained by an influence of stratospheric air only. Supported by simulations from the *p*-TOMCAT tropospheric chemical transport model (Yang et al., 2010), we have investigated more systematically the relationship between high retrieved tropospheric BrO columns and low tropopause heights in the polar region, and we found a plausible explanation for it by considering the release of bromine through the production of sea salt aerosols during blowing snow events (linked to low pressure systems). However, no firm conclusions can be drawn from our analysis on the relative importance of such mechanism on the polar bromine explosion events. Outside the polar region, it is found that the tropospheric BrO columns retrieved using our algorithm are consistent with the presence of a global BrO background at free tropospheric altitudes, with columns of 1-3 $\times 10^{13}$ molec cm^{-2}, in agreement with results from other studies.

Acknowledgements. This research has been financially supported through the Belgium Prodex 9 contract SECPEA, the EUMETSAT O3M-SAF Continuous Development and Operation Project, the GEOmon (FP6-2005-Global-4-036677) and SHIVA (226224-FP7-ENV-2008-1) projects from the European Commission. The authors acknowledge EUMETSAT for providing the GOME-2 level-1 data product and DLR-IMF for providing the GOME-2 operational product.

Edited by: J. W. Bottenheim

References

Afe O. T., Richter, A., Sierk, B., Wittrock, F., and Burrows, J. P.: BrO emissions from volcanoes: a survey using GOME and SCIAMACHY measurements, Geophys. Res. Lett., 31, L24113, doi:10.1029/2004GL0200994, 2004.

Aliwell, S. R., Van Roozendael, M., Johnston, P. V., Richter, A., Wagner, T., Arlander, D.W., Burrows, J. P., Fish, D. J., Jones, R. L., Tornkvist, K. K., Lambert, J. C., Pfeilsticker, K., and Pundt, I.: Analysis for BrO in zenith-sky spectra: An intercomparison exercise for analysis improvement, J. Geophys. Res., 107, D140, doi:10.1029/2001JD000329, 2002.

Begoin, M., Richter, A., Weber, M., Kaleschke, L., Tian-Kunze, X., Stohl, A., Theys, N., and Burrows, J. P.: Satellite observations of long range transport of a large BrO plume in the Arctic,

Atmos. Chem. Phys., 10, 6515–6526, doi:10.5194/acp-10-6515-2010, 2010.

Bobrowski, N., Hönninger, G., Galle, B., and Platt, U.: Detection of bromine monoxide in a volcanic plume, Nature, 423, 273–276, 2003.

Boersma, K. F., Eskes, H. J., and Brinksma, E. J.: Error analysis for tropospheric NO_2 retrieval from space, J. Geophys. Res., 109, D04311, doi:10.1029/2003JD003962, 2004.

Bogumil, K., Orphal, J., Homann, T., Voigt, S., Spietz, P., Fleischmann, O.C., Vogel, A., Hartmann, M., Bovensmann, H., Frerik, J., and Burrows, J. P.: Measurements of molecular absorption spectra with the SCIAMACHY Pre-Flight Model: Instrument characterization and reference spectra for atmospheric remote sensing in the 230–2380 nm region, J. Photochem. Photobiol. A, 157, 167–184, 2003.

Bovensmann, H., Burrows, J. P., Buchwitz, M., Frerick, J., Noël, S., Rozanov, V. V., Chance, K. V., Goede, A. P. H.: SCIAMACHY: Mission objectives and Measurement Modes, J. Atm. Sci., 56, 127–150, 1999.

Brion, J., Chakir, A., Daumont, D., and Malicet, J.: High-resolution laboratory absorption cross sections of O_3, Temperature effect, Chem. Phys. Lett., 213(5–6), 610–612, 1993.

Burrows, J. P., Dehn, A., Deters, B., Himmelmann, S., Richter, A., Voigt, S., and Orphal, J.: Atmospheric Remote-Sensing Reference Data from GOME: 1. Temperature-Dependent Absorption Cross Sections of NO_2 in the 231–794 nm Range, J. Quant. Spectrosc. Radiat. Transfer, 60, 1025–1031, 1998.

Chance, K.: Analysis of BrO measurements from the Global Ozone Monitoring Experiment, Geophys. Res. Lett., 25, 3335–3338, 1998.

De Smedt, I., Müller, J.-F., Stavrakou, T., van der A, R., Eskes, H., and Van Roozendael, M.: Twelve years of global observations of formaldehyde in the troposphere using GOME and SCIAMACHY sensors, Atmos. Chem. Phys., 8, 4947–4963, doi:10.5194/acp-8-4947-2008, 2008.

Dorf, M., Butz, A., Camy-Peyret, C., Chipperfield, M. P., Kritten, L., and Pfeilsticker, K.: Bromine in the tropical troposphere and stratosphere as derived from balloon-borne BrO observations, Atmos. Chem. Phys., 8, 7265–7271, doi:10.5194/acp-8-7265-2008, 2008

Errera, Q., Daerden, F., Chabrillat, S., Lambert, J. C., Lahoz, W. A., Viscardy, S., Bonjean, S., and Fonteyn, D.: 4D-Var assimilation of MIPAS chemical observations: ozone and nitrogen dioxide analyses, Atmos. Chem. Phys., 8, 6169–6187, doi:10.5194/acp-8-6169-2008, 2008.

EUMETSAT, GOME-2 FM3 Calibration: Instrument Performance Testing, MO-TR-TPD-GO-0094, 2009.

Fitzenberger, R., Bösch, H., Camy-Peyret, C., Chipperfield, M. P., Harder, H., Platt, U., Sinnhuber, B.-M., Wagner, T., and Pfeilsticker, K.: First profile measurements of tropospheric BrO, Geophys. Res. Lett., 27, 2921–2924, 2000.

Fleischmann, O. C., Hartmann, M., Burrows J. P., and Orphal, J.: New ultraviolet absorption cross-sections of BrO at atmospheric temperatures measured by time-windowing Fourier transform spectroscopy, J. Photochem. Photobiol. A, 168, 117–132, 2004.

Frieß, U., Hollwedel, J., König-Langlo, G., Wagner, T., and Platt, U.: Dynamics and chemistry of tropospheric bromine explosion events in the Antarctic coastal region, J. Geophys. Res., 109, D06305, doi:10.1029/2003JD004133, 2004.

Grainger, J. F. and Ring, J.: Anomalous Fraunhofer lines profiles, Nature, 193, p. 762, 1962.

Harder, H., Camy-Peyret, C., Ferlemann, F., Fitzenberger, R., Hawat, T., Osterkamp, H., Perner, D., Platt, U., Schneider, M., Vradelis, P., and Pfeilsticker, K.: Stratospheric BrO Profiles Measured at Different Latitudes and Seasons: Atmospheric Observations, Geophys. Res. Lett., 25, 3843–3846, 1998.

Hausmann, M. and Platt, U.: Spectroscopic measurement of bromine oxide and ozone in the high Arctic during Polar Sunrise Experiment 1992, J. Geophys. Res., 99, 25399–25414, 1994.

Hebestreit, K., Stutz, J., Rosen, D., Matveiv, V., Peleg, M., Luria, M., and Platt, U.: DOAS measurements of tropospheric bromine oxide in mid-latitudes, Science, 283, 55–57, 1999.

Hendrick, F., Van Roozendael, M., Chipperfield, M. P., Dorf, M., Goutail, F., Yang, X., Fayt, C., Hermans, C., Pfeilsticker, K., Pommereau, J.-P., Pyle, J. A., Theys, N., and De Mazire, M.: Retrieval of stratospheric and tropospheric BrO profiles and columns using ground-based zenith-sky DOAS observations at Harestua, 60° N, Atmos. Chem. Phys., 7, 4869–4885, doi:10.5194/acp-7-4869-2007, 2007.

Hendrick, F., Johnston, P. V., De Mazière, M., Fayt, C., Hermans, C., Kreher, K., Theys, N., and Van Roozendael, M.: One-decade trend analysis of stratospheric BrO over Harestua (60° N) and Lauder (45° S) reveals a decline, Geophys. Res. Lett., 35, L14801, doi:10.1029/2008GL034154, 2008.

Hendrick, F., Rozanov, A., Johnston, P. V., Bovensmann, H., De Mazière, M., Fayt, C., Hermans, C., Kreher, K., Lotz, W., Sinnhuber, B.-M., Theys, N., Thomas, A., Burrows, J. P., and Van Roozendael, M.: Multi-year comparison of stratospheric BrO vertical profiles retrieved from SCIAMACHY limb and ground-based UV-visible measurements, Atmos. Meas. Tech., 2, 273–285, doi:10.5194/amt-2-273-2009, 2009.

Hollwedel, J.: Observations of Tropospheric and Stratospheric Bromine Monoxide from Satellite, PhD. Thesis, University of Heidelberg, Germany, 2005.

Hönninger, G. and Platt, U.: Observations of BrO and its vertical distribution during surface ozone depletion at Alert, Atmos. Environ., 36, 2481–2489, 2002.

Jones, A. E., Anderson, P., Begoin, M., Brough, N., Hutterli, M., Marshall, G., Richter, A., Roscoe, H., and Wolff, E.: BrO, blizzards, and drivers of polar tropospheric ozone depletion events, Atmos. Chem. Phys., 9, 4639–4652, 2009, http://www.atmos-chem-phys.net/9/4639/2009/.

Jones, A. E., Anderson, P., Wolff, E., Roscoe, H., Marshall, G., Richter, A., Brough, N., and Colwell, S.: Vertical structure of Antarctic tropospheric ozone depletion events: characteristics and broader implications, Atmos. Chem. Phys., 10, 7775–7794, 2010, http://www.atmos-chem-phys.net/10/7775/2010/.

Kaleschke, L., Richter, A., Burrows, J. P., Afe, O., Heygster, G., Notholt, J., Rankin, A.M., Roscoe, H.K., Hollwedel, J., Wagner, T., and Jacobi, H.-W.: Frost flowers on sea ice as a source of sea salt and their influence on tropospheric halogen chemistry, Geophys. Res. Lett., 31, L16114, doi:10.1029/2004GL020655, 2004.

Koelemeijer, R. B. A., Stammes, P., Hovenier, J. W., and de Haan, J. F.: Global distributions of effective cloud fraction and cloud top pressure derived from oxygen A band spectra measured by the Global Ozone Monitoring Experiment: com-

parison to ISCCP data, J. Geophys. Res., 107(D12), 4151, doi:10.1029/2001JD000840, 2002.

Koelemeijer, R. B. A., de Haan, J. F., and Stammes, P.: A database of spectral surface reflectivity in the range 335–772 nm derived from 5.5 years of GOME observations, J. Geophys. Res.-Atm., 108(D2), 4070, doi:10.1029/2002JD002429, 2003.

Kreher, K., Johnston, P. V., Wood, S. W., Nardi, B., and Platt, U.: Ground-based measurements of tropospheric and stratospheric BrO at Arrival Heights, Antarctica, Geophys. Res. Lett., 24, 3021–3024, 1997.

Lary, D. J.: Gas phase atmospheric bromine photochemistry, J. Geophys. Res., 101, 1505–1516, 1996.

Lary, D. J.: Halogens and the chemistry of the free troposphere, Atmos. Chem. Phys., 5, 227–237, doi:10.5194/acp-5-227-2005, 2005.

Leser, H., Höninger, G., and Platt, U.: Max-DOAS measurements of BrO and NO_2 in the marine boundary layer, Geophys. Res. Lett., 30, 1537, doi:10.1029/2002GL015811, 2003.

Martin, R. V., Chance, K., Jacob, D. J., Kurosu, T. P., Spurr, R. J. D., Bucsela, E., Gleason, J.F., Palmer, P. I., Bey, I., Fiore, A. M., Li, Q., Yantosca, R. M., and Koelemeijer, R. B. A.: An improved retrieval of tropospheric nitrogen dioxide from GOME, J. Geophys. Res., 107(D20), 4437, doi:10.1029/2001JD001027, 2002.

Mayer, B. and Kylling, A.: Technical note: The libRadtran software package for radiative transfer calculations - description and examples of use, Atmos. Chem. Phys., 5, 1855–1877, doi:10.5194/acp-5-1855-2005, 2005.

McConnel, J. C., Henderson, G. S., Barrie, L., Bottenheim, J., Niki, H., Langford, C. H., and Templeton, E. M. J.: Photochemical bromine production implicated in Arctic boundary-layer ozone depletion, Nature, 355, 150–152, 1992.

McElroy, M. B., Salawitch, R. J., Wofsy, S. C., and Logan, J. A.: Reductions of Antarctic ozone due to synergetic interactions of chlorine and bromine, Nature, 321, 759–762, 1986.

Meller, R. and Moortgat, G. K.: Temperature dependence of the absorption cross-section of HCHO between 223 and 323 K in the wavelength range 225–375 nm, J. Geophys. Res., 105(D6), 7089–7102, doi:10.1029/1999JD901074, 2000.

Montzka, S. A., Butler, J. H., Hall, B. D., Mondeel, D. J., and Elkins, J. W.: A decline in tropospheric organic bromine, Geophys. Res. Lett., 30(15), 1826, doi:10.1029/2003GL017745, 2003.

Munro, R., Eisinger, M., Anderson, C., Callies, J., Corpaccioli, E., Lang, R., Lefebvre, A., Livschitz, Y., and Albinana, A. P.: GOME-2 on MetOp, in: Proc. of The 2006 EUMETSAT Meteorological Satellite Conference, Helsinki, Finland, 12–16 June 2006, EUMETSAT, p. 48, 2006.

Neuman, J. A., Nowak, J. B., Huey, L. G., Burkholder, J. B., Dibb, J. E., Holloway, J. S., Liao, J., Peischl, J., Roberts, J. M., Ryerson, T. B., Scheuer, E., Stark, H., Stickel, R. E., Tanner, D. J., and Weinheimer, A.: Bromine measurements in ozone depleted air over the Arctic Ocean, Atmos. Chem. Phys., 10, 6503–6514, doi:10.5194/acp-10-6503-2010, 2010.

Oppenheimer, C., Tsanev, V. I., Braban, C. F, Cox, R. A., Adams, J. W., Aiuppa, A., Bobrowski, N., Delmelle, P., Barclay, J., and McGonigle, A. J.: BrO formation in volcanic plumes, Geochim. Cosmochim. Acta, 70, 2935–2941, 2006.

Palmer, P. I., Jacob, D. J., Chance, K., Martin, R. V., Spurr, R. J. D., Kurosu, T. P., Bey, I., Yantosca, R., Fiore, A., and Li, Q.: Air-mass factor formulation for spectroscopic measurements from satellites: application to formaldehyde retrievals from GOME, J. Geophys. Res., 106(D13), 14539–14550, doi:10.1029/2000JD900772, 2001.

Platt, U. and Stutz, J.: Differential Optical Absorption Spectroscopy (DOAS), Principle and Applications, ISBN 3-340-21193-4, Springer Verlag, Heidelberg, Germany, 2008.

Read, K. A., Mahajan, A. S., Carpenter, L. J., Evans, M. J., Faria, B. V. E., Heard, D. E., Hopkins, J. R., Lee, J. D., Moller, S. J., Lewis, A. C., Mendes, L., McQuaid, J. B., Oetjen, H., Saiz-Lopez, A., Pilling, M. J., and Plane, J. M. C.: Extensive halogen-mediated ozone destruction over the tropical Atlantic Ocean, Nature, 453, 1232–1235, 2008.

Richter, A.: Absorptionspektroskopische Messungen stratosphärischer Spurengase über Bremen, 55° N, PhD thesis, Inst. für Umweltphysik, Univ. of Bremen, Bremen, Germany, 1997.

Richter, A., Wittrock, F., Eisinger, M., and Burrows, J. P.: GOME Observations of Tropospheric BrO in Northern Hemispheric Spring and Summer 1997, Geophys. Res. Lett., 25, 2683–2686, 1998.

Richter, A., Wittrock, F., Ladstätter-Weissenmayer, A., and Burrows, J. P.: GOME measurements of stratospheric and tropospheric BrO, Adv. Space Res., 29, 1667–1672, 2002.

Richter, A., Burrows, J. P., Nüß, H., Granier, C, and Niemeier, U.: Increase in tropospheric nitrogen dioxide over China observed from space, Nature, 437, 129-132, doi:10.1038/nature04092, 2005.

Rodgers, C. D.: Inverse Methods for Atmospheric Sounding, Theory and Practice, World Scientific Publishing, Singapore, New-Jersey, London, Hong Kong, 2000.

Rozanov, A., Rozanov, V., and Burrows, J. P.: A numerical radiative transfer model for a spherical planetary atmosphere: Combined differential integral approach involving the Piccard iterative approximation, J. Quant. Spectrosc. Radiat. Transfer, 69, 491–512, 2001.

Saiz-Lopez, A., Plane, J. M. C., and Shilito, J. A.: Bromine oxide in the mid-latitude marine boundary layer, Geophys. Res. Lett., 31, L03111, doi:10.1029/2003GL018956, 2004.

Salawitch, R. J., Canty, T., Kurosu, T., Chance, K., Liang, Q., da Silva, A., Pawson, S., Nielsen, J. E., Rodriguez, J. M., Bhartia, P. K., Liu, X., Huey, L. G., Liao, J., Stickel, R. E., Tanner, D. J., Dibb, J. E., Simpson, W. R., Donohoue, D., Weinheimer, A., Flocke, F., Knapp, D., Montzka, D., Neuman, J. A., Nowak, J. B., Ryerson, T. B., Oltmans, S., Blake, D. R., Atlas, E. L., Kinnison, D. E., Tilmes, S., Pan, L. L., Hendrick, F., Van Roozendael, M., Kreher, K., Johnston, P. V., Gao, R. S., Johnson, B., Bui, T. P., Chen, G., Pierce, R. B., Crawford, J. H., and Jacob, D. J: A new interpretation of total column BrO during Arctic Spring, Geophys. Res. Lett. (Frontier Articles), 37, L21805, doi:10.1029/2010GL043798, 2010.

Schoeberl, M. R.: Extratropical stratosphere-troposphere mass exchange, J. Geophys. Res., 109, D13303, doi:10.1029/2004JD004525, 2004.

Schofield, R., Kreher, K., Connor, B. J., Johnston, P. V., Thomas, A., Shooter, D., Chipperfield, M. P., Rodgers, C. D., and Mount, G. H.: Retrieved tropospheric and stratospheric BrO columns over Lauder, New Zealand., J. Geophys. Res., 109, D14304,

doi:10.1029/2003JD004463, 2004.

Schofield, R., Johnston, P. V., Thomas, A., Kreher, K., Connor, B. J., Wood, S., Shooter, D., Chipperfield, M. P., Richter, A., von Glasow, R., and Rodgers, C. D.: Tropospheric and stratospheric BrO columns over Arrival Heights, Antartica, 2002, J. Geophys. Res., 111, D22310, doi:10.1029/2005JD007022, 2006.

Schroeder, W. H., Anlauf, K. G., Barrie, L. A., Lu, J. Y., Steffen, A., Scheenberger, D. R., and Berg, T.: Arctic springtime depletion of mercury, Nature, 394, 331–332, 1998.

Siddans, R., Latter, B. G., Kerridge, B. J., Smeets, J., Otter, G., and Slijkhuis, S.: Analysis of GOME-2, Slit function Measurements Final Report, Eumetsat Contract No. EUM/CO/04/1298/RM, 2006.

Simpson, W. R., von Glasow, R., Riedel, K., Anderson, P., Ariya, P., Bottenheim, J., Burrows, J., Carpenter, L. J., Frieß, U., Goodsite, M. E., Heard, D., Hutterli, M., Jacobi, H.-W., Kaleschke, L., Neff, B., Plane, J., Platt, U., Richter, A., Roscoe, H., Sander, R., Shepson, P., Sodeau, J., Steffen, A., Wagner, T., and Wolff, E.: Halogens and their role in polar boundary-layer ozone depletion, Atmos. Chem. Phys., 7, 4375–4418, doi:10.5194/acp-7-4375-2007, 2007.

Sinnhuber, B.-M., Rozanov, A., Sheode, N., Afe, O. T., Richter, A., Sinnhuber, M., Wittrock, F., Stiller, G. P., von Clarmann, T., Linden, A., and Burrows, J. P.: Global observations of stratospheric bromine monoxide from SCIAMACHY, Geophys. Res. Lett., 32, L20810, doi:10.1029/2005GL023839, 2005.

Sirois, A. and Barrie, L.: Arctic lower tropospheric aerosol trends and composition at Alert, Canada: 1980–1995, J. Geophys. Res., 104(D9), 11599–11618, 1999.

Theys, N., Van Roozendael, M., Hendrick, F., Fayt, C., Hermans, C., Baray, J.-L., Goutail, F., Pommereau, J.-P., and De Mazire, M.: Retrieval of stratospheric and tropospheric BrO columns from multi-axis DOAS measurements at Reunion Island (21° S, 56° E), Atmos. Chem. Phys., 7, 4733–4749, doi:10.5194/acp-7-4733-2007, 2007.

Theys, N., Van Roozendael, M., Dils, B., Hendrick, F., Hao, N., and De Mazière, M.: First satellite detection of volcanic bromine monoxide emission after the Kasatochi eruption, Geophys. Res. Lett., 36, L03809, doi:10.1029/2008GL036552, 2009a.

Theys, N., Van Roozendael, M., Errera, Q., Hendrick, F., Daerden, F., Chabrillat, S., Dorf, M., Pfeilsticker, K., Rozanov, A., Lotz, W., Burrows, J. P., Lambert, J.-C., Goutail, F., Roscoe, H. K., and De Mazière, M.: A global stratospheric bromine monoxide climatology based on the BASCOE chemical transport model, Atmos. Chem. Phys., 9, 831–848, 2009b, http://www.atmos-chem-phys.net/9/831/2009/.

Van Roozendael, M., Wagner, T., Richter, A., Pundt, I., Arlander, D., Burrows, J. P., Chipperfield, M., Fayt, C., Johnston, P. V., Lambert, J.-C., Kreher, K., Pfeilsticker, K., Platt, U., Pommereau, J.-P., Sinnhuber, B.-M., Tornkvist, K. K., and Wittrock, F.: Intercomparison of BrO measurements from ERS-2 GOME, ground-based and balloon platforms , Adv. Space Res., 29, 1661–1666, 2002.

Van Roozendael, M., De Smedt, I., Fayt, C., Wittrock, F., Richter, A., Afe, O.: First validation of SCIAMACHY BrO columns, in Proc. Second Workshop on the Atmospheric Chemistry Validation of ENVISAT (ACVE-2), Frascati, Italy, 3–7 May, 2004.

Viscardy, S., Errera, Q., Christophe, Y., Chabrillat, S., and Lambert, J.-C.: Evaluation of ozone analysis from UARS MLS assimilation by BASCOE between 1992 and 1997, JSTARS 3, 190–202, 2010.

Vogt, R., Crutzen, P. J., and Sander, P.: A mechanism for halogen release from sea-salt aerosol in the remote marine boundary layer, Nature, 383, 327–330, 1996.

von Glasow, R. and Crutzen, P. J.: Tropospheric Halogen Chemistry, Vol. 4.02, in: Treatise on Geochemistry Update 1, edited by: Holland, H. D. and Turekian, K. K., Elsevier-Pergamon, Oxford, UK, 1–67, 2007.

von Glasow, R., von Kuhlmann, R., Lawrence, M. G., Platt, U., and Crutzen, P. J.: Impact of reactive bromine chemistry in the troposphere, Atmos. Chem. Phys., 4, 2481–2497, doi:10.5194/acp-4-2481-2004, 2004.

Vountas, M., Rozanov, V. V., and Burrows, J. P.: Ring effect: Impact of rotational raman scattering on radiative transfer in earth's atmosphere, J. Quant. Spectrosc. Radiat. Transfer., 60, 943–961, 1998.

Wagner, T. and Platt, U.: Satellite mapping of enhanced BrO concentrations in the troposphere, Nature, 395, 486–490, 1998.

Wagner, T., Leue, C., Wenig, M., Pfeilsticker, K., and Platt, U.: Spatial and temporal distribution of enhanced boundary layer BrO concentrations measured by the GOME instrument aboard ERS-2, J. Geophys. Res., 106, 24225–24236, 2001.

Wang, P., Stammes, P., van der A, R., Pinardi, G., and van Roozendael, M.: FRESCO+: an improved O_2 A-band cloud retrieval algorithm for tropospheric trace gas retrievals, Atmos. Chem. Phys., 8, 6565–6576, doi:10.5194/acp-8-6565-2008, 2008.

Wennberg, P.: Atmospheric chemistry: Bromine explosion, Nature, 397, 299–301, 1999.

World Meteorological Organization (WMO): Scientific Assessment of Ozone Depletion: 2006, Global ozone research and monitoring project, Chapter 2: Halogenated Very Short-Lived Substances, Rep. 50, Geneva, Switzerland, 2007.

Yang, X., Cox, R. A., Warwick, N. J., Pyle, J. A., Carver, G. D., O'Connor, F. M., and Savage, N. H.: Tropospheric bromine chemistry and its impacts on ozone: A model study, J. Geophys. Res., 110, D23311, doi:10.1029/2005JD006244, 2005.

Yang, X., Pyle, J. A., and Cox, R. A.: Sea salt aerosol production and bromine release: Role of snow on sea ice, Geophys. Res. Lett., 35, L16815, doi:10.1029/2008GL034536, 2008.

Yang, X., Pyle, J. A., Cox, R. A., Theys, N., and Van Roozendael, M.: Snow-sourced bromine and its implications for polar tropospheric ozone, Atmos. Chem. Phys., 10, 7763–7773, doi:10.5194/acp-10-7763-2010, 2010.

Ziemke, J. R., Chandra, S., and Bhartia, P. K.: "Cloud slicing": A new technique to derive upper tropospheric ozone from satellite measurements, J. Geophys. Res., 106(D9), 9853–9867, 2001.